COMPARATIVE STUDY OF DIFFERENTIATION AND INTEGRATION TECHNIQUES FOR FEEDBACK CONTROL SYSTEMS

JING LIU

Bachelor of Science in the Department of Control Engineering

Harbin Institute of Technology, P.R. China

July 1994

Submitted in partial fulfillment of requirements for the degree

MASTER OF SCEINCE

CLEVELAND STATE UNIVERSITY

December, 2002

This thesis has been approved

For the Department of Electrical and Computer Engineering

And the College of Graduate Studies by

_____

Thesis Committee Chairperson, Dr. Zhiqiang Gao

Department of Electrical and Computer Engineering, December 12, 2002

_____

Thesis Committee Member, Dr. James H. Burghart

Department of Electrical and Computer Engineering, December 12, 2002

_____

Thesis Committee Member, Dr. Dan Simon

Department of Electrical and Computer Engineering, December 12, 2002

DEDICATION

To my parents, my husband and my son

It is their anticipation that stimulates me to pursue higher education!

ACKNOWLEDGMENT

First, I would like to express my deepest appreciation to my advisor, Dr. Zhiqiang Gao, for his supervision and help throughout the course of my study. It was an invaluable experience working in his applied control research laboratory and learning from his problem-solving methodology and approach to research.

I would like to thank Dr. James H. Burghart and Dr. Dan Simon, who are on my committee, for their time in reading and evaluating this thesis.

I would also like to thank my friends, Weiwen Wang, Minshao Zhu, and Shahid Parvez, Bosheng Sun, Zhan Ping, Rob, Chunming Yang, Tong Ren and the rest of the electrical engineering department at Cleveland State University for the endless support given to me while at Cleveland State University.

A special thanks is to my family for their continuous support, encouragement, and inspiration to finish my degree.

COMPARATIVE STUDY OF DIFFERENTIATION AND INTEGRATION TECHNIQUES FOR FEEDBACK CONTROL SYSTEMS

Jing Liu

Abstract

The proportional-integral-derivative (PID) controller is an important technology because it is used in over 95% of current industrial control applications. The improvement of PID will have significant impacts on control practice and is therefore of great interest to researchers. To this end, there have been many alternative differentiation and integration techniques proposed in the literature or used by practicing engineers. The main purpose in this research is to determine, out of the proposed alternatives, which ones offer the best practical solutions. In particular, the linear approximation differentiators, the nonlinear and linear Tracking Differentiators, the First Order Robust Exact Differentiator and the observer-based differentiator are studied to determine which one provides the best approximation of the differentiation signal under noisy conditions. The nonlinear integrator, the Clegg integrator and the modified nonlinear integrator are also compared with the pure integrator in terms of phase lag and performance in simulation. Finally, various differentiation technologies are evaluated in an industrial motion control example and various integration technologies are evaluated in a DC-DC power converter application.

Keywords: PID, Linear Approximation Differentiator, Tracking Differentiator, Observer, Nonlinear Integrator, Clegg Integrator

TABLE OF CONTENTS

LIST OF FIGURES

Figure **Page**

LIST OF TABLES

Table **Page**

CHAPTER I

INTRODUCTION

The Proportional-Integral-Derivative (PID) controller was first described by N. Minorsky in 1922 [12]. Today, it is still the tool of choice in over 95% of current industrial control applications. The goal of feedback control is to drive the error between the output of the process, also called plant, and its desired value to zero as quickly as possible subject to the physical constraints. In the three parts of PID, the proportional control usually plays the main role and the integral control helps to achieve zero steady-state error; the derivative control is useful in avoiding overshoot in responses. The PID controller is easy to understand and simple to implement,but due to its limited design parameters, the performance of PID is somewhat limited compared to other techniques. The improvement of the differentiation and integration techniques is the key in enhancing the PID performance.

1.1 Motivation

The primary issue in differentiation is the noise corruption. It is well known that a pure differentiator is not physically realizable due to its noise amplification property.

Various approximations of the pure differentiation have been proposed. Finding an approximation differentiator with good noise immunity is paramount in achieving high control performance. The integration element in PID introduces another adverse phenomenon, namely the phase lag of 90°. It is well known that this phase lag reduces stability margins and could even destabilize the closed-loop system. Therefore, in general, the phase lag should be avoided as much as possible, particularly in the frequency range close to the bandwidth of the closed-loop system.

There have been many variations of differentiation and integration techniques proposed in the literature, which is reviewed below. The research that led to this thesis is driven primarily by the desire to find the best and, yet, practical differentiation and integration techniques. It is anticipated that the resulting conclusions will have a significant impact in PID control design in practical control application.

1.2 **Literature Review**

To achieve better performance, differentiation and integration techniques were proposed over the years [1, 3-8, 17]. In the area of differentiation technique, the following methods are proposed:

1) The method of linear differentiator construction is a pure differentiator appended with a low-pass filter that is used to damp noises [5-7]. Stochastic features of the signal and the noise are also considered [8].
2) In recent years, the nonlinear Tracking Differentiator has been proposed which is based on the time optimal synthesis theory and the time scale concept of the singularly perturbed systems theory [1].

3) The Robust Exact Differentiator, which is based on the sliding mode, was also proposed [3].

4) The differentiated signal can also be abstracted from the state observer.

In this thesis, we will try to determine which one of these techniques has the best performance. The answer to this question goes a long way in helping practicing engineers improve the performance of control systems.

In terms of the integration technique, the two key techniques that are frequently researched are: the nonlinear integrator that is based on the nonlinear theory [4], and the Clegg Integrator whose output resets to zero whenever its input crosses zero [17]. A systematic comparison of these two methods is needed.

1.3 Thesis Outline

The mathematical models of differentiation technologies are presented in Chapter II. The differentiators' responses in time-domain and analysis in frequency-domain are presented in Chapter III. Then different differentiators are put together, whose responses are compared based on the step response of a standard linear second order system in time domain. Specifically, the NTD and LA2 are compared with a Linear State Observer and a Nonlinear State Observer. As an extension, the performances of double differentiators and ESO are also compared in section 3.3. The result of the comparison is described. Four kinds of integrators are presented in Chapter IV. They are analyzed using a describing function and compared in the PWM DC-DC power converter. A motion control system is described in Chapter V. An advanced control law is proved. In this

application, differentiators also are evaluated. Finally, conclusions and recommendation about some future improvements and application prospects are given in Chapter VI.

CHAPTER II

DIFFERENTIATION TECHNIQUES

In this chapter, the classical linear approximation differentiators (LAD), the nonlinear and linear Tracking Differentiators (NTD and LTD), the first order Robust Exact Differentiator (RED) and the observer-based differentiators (OBD) are introduced. Their mathematical descriptions are presented.

2.1 Classical Linear Approximation Differentiators

A differentiator has an input *u(t)* and an output *y(t)* described in the diagram below.

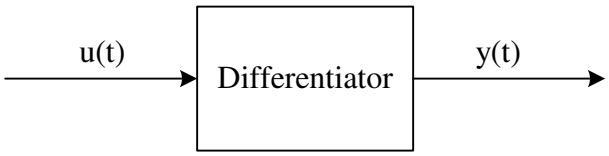

Figure 1. The relationship of differentiator's input and output

The pure differentiator is defined as:

$$y(t) = \dot{u}(t) = \frac{du(t)}{dt} \tag{2.1.1}$$

Since the pure differentiator is susceptible to noises, most differentiators used today are approximations. They satisfy $y(t) \approx \dot{u}(t)$ in some sense. In general, a pure differentiator and its linear approximation can be described as:

$$G(s) = \frac{s}{(\tau s + 1)^m} \qquad m = 0, 1, 2, ... \tag{2.1.2}$$

For *m*=0, it is a pure differentiator which is not physically realizable. For *m*=1, it is a first-order linear approximation differentiator (LA1). The output *Y(s)* can be derived from:

$$Y(s) = \frac{s}{\tau s + 1} U(s) \tag{2.1.3}$$

It can be rewritten as:

$$Y(s) = \frac{1}{\tau}(1 - \frac{1}{\tau s + 1}) U(s) = \frac{1}{\tau}(U(s) - \frac{U(s)}{\tau s + 1}) \tag{2.1.4}$$

In the time domain, the relationship of *y(t)* and *u(t)* is:

$$y(t) = \frac{1}{\tau}(u(t) - \bar{u}(t)), \qquad \dot{\bar{u}}(t) = -\frac{1}{\tau}(\bar{u}(t) - u(t)) \tag{2.1.5}$$

When time constant τ is very small, $\bar{u}(t)$ tracks input signal *u(t)* very quickly. But it has time delay and this time delay is equal to τ because $\frac{1}{\tau s + 1} \approx e^{-\tau s}$. Therefore $\bar{u}(t) \approx u(t - \tau)$, and

$$y(t) = \frac{1}{\tau}(u(t) - \bar{u}(t)) \approx \frac{1}{\tau}(u(t) - u(t - \tau)) \approx \dot{u}(t) \tag{2.1.6}$$

The smaller the time constant τ, the closer the output signal *y(t)* is to the differential signal $\dot{u}(t)$.

If white noise *n(t)* is added to the input signal *u(t)*, equation (2.1.5) will change to

$$y(t) = \frac{1}{\tau}(u(t) + n(t) - \bar{u}(t)), \qquad \dot{\bar{u}}(t) = -\frac{1}{\tau}(\bar{u}(t) - u(t) + n(t)) \tag{2.1.7}$$

If the time constant τ is not very small, the second equation is a good low pass filter. It can filter out the effect of noise *n(t)* and $\bar{u}(t)$ still satisfies $\bar{u}(t) \approx u(t-\tau)$, therefore the output will be

$$y(t) = \frac{1}{\tau}(u(t) - u(t-\tau)) + \frac{n(t)}{\tau} \approx \dot{u}(t) + \frac{1}{\tau}n(t) \tag{2.1.8}$$

It means the output signal *y(t)* equals the differential signal of input *u(t)* plus the noise signal which is amplified $\frac{1}{\tau}$ times. So when τ goes smaller, the noise is amplified. To attenuate the effect of noise, a higher-order linear approximation is used, i.e., *m* = 2,3, …. The noise attenuation effects can be observed from the Bode plot of *G(s)* in Figure 2. The higher the *m*, the better the noise attenuation.

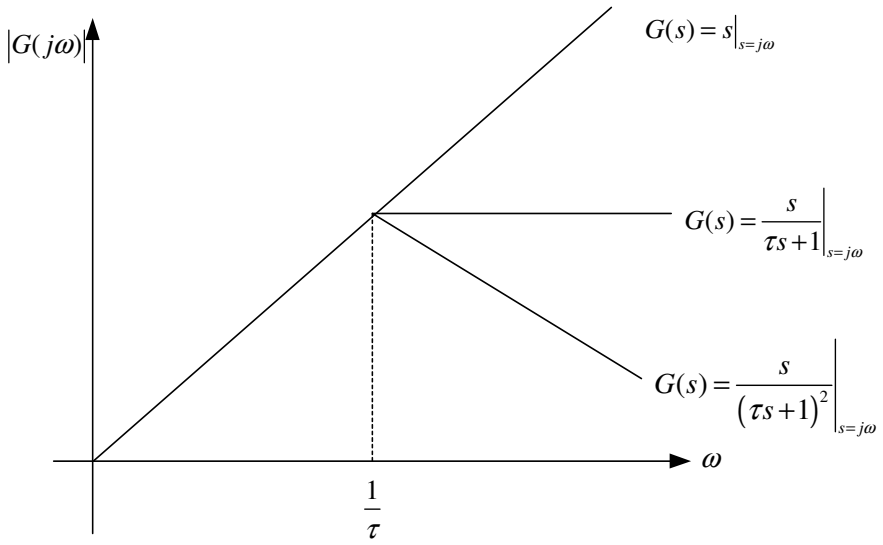

Figure 2. Filter performance of different order LAD

Another form of LAD is

$$G(s)=\frac{1}{\tau_2-\tau_1}(\frac{1}{\tau_1 s+1}-\frac{1}{\tau_2 s+1}) \tag{2.1.9}$$

When $\tau_1=\tau_2=\tau$, m=2, equation (2.1.9) is equivalent to equation (2.1.2). It is similar to the second-order linear approximation differentiator (LA2).

For m=3, equation (2.1.2) is a third-order linear approximation differentiator (LA3).

2.2 Tracking Differentiators

There are two kinds of Tracking Differentiators, nonlinear and linear. The Nonlinear Tracking Differentiator (NTD) [1] is inspired from the time optimal synthesis theory and the time scale concept of the singularly perturbed system theory. The Linear Tracking Differentiator (LTD) [2] is based on the similar idea with second-order classical differentiator. Both of them can track input signals and get a differential signal via choosing suitable tracking parameters at the same time.

Consider a second-order cascaded integrator from an arbitrary initial state

$$\begin{cases}\dot{x}_1 = x_2 \\ \dot{x}_2 = v, \quad |v| \le R\end{cases} \tag{2.2.1}$$

For the states to reach the origin in minimum time, the time-optimal control law is given as [18]

$$v(x_1, x_2) = -Rsign(x_1 + \frac{x_2|x_2|}{2R}) \tag{2.2.2}$$

where *sign(x)* is defined as

$$sign(x)=\begin{cases}1 & x>0\\ 0 & x=0\\ -1 & x<0\end{cases}$$

Combining (2.2.1) and (2.2.2), the closed-loop system is

$$\begin{cases}\dot{x}_1 = x_2\\ \dot{x}_2 = -Rsign(x_1+\dfrac{x_2|x_2|}{2R})\end{cases} \tag{2.2.3}$$

Replacing x_1 with $x_1-u(t)$, the equation (2.2.3) becomes

$$\begin{cases}\dot{x}_1 = x_2\\ \dot{x}_2 = -Rsign(x_1-u(t)+\dfrac{x_2|x_2|}{2R})\end{cases} \tag{2.2.4}$$

which is denoted as the Nonlinear Tracking Differentiator (NTD) [1]. Here *R* represents the maximum acceleration the system can attain and is a function of the maximum actuation available in the system. $x_1(t)$ and $x_2(t)$ are the state variables, *u(t)* is the input signal. It was shown [1] that $x_1(t)$ converges to *u(t),* and that $x_2(t)$, which is the derivative of $x_1(t)$, is the generalized derivative of *u(t).* Since $x_2(t)$ is obtained through integration, it is a kind of differentiation with good signal to noise ratio.

The NTD can be converted to discrete form using Euler's method, which yields

$$\begin{cases}x_1(k+1) = x_1(k)+hx_2(k)\\ x_2(k+1) = x_2(k)-hRsign(x_1(k)-u(k)+\dfrac{x_2(k)|x_2(k)|}{2R})\end{cases} \tag{2.2.5}$$

where *h* is the step size. For smoothness of the output signal, the sign function *sign* can be changed to the linear saturate function *sat*, i.e.

$$\begin{cases} x_1(k+1) = x_1(k) + hx_2(k) \\ x_2(k+1) = x_2(k) - hRsat(a,\delta) \\ a = x_1(k) - u(k) + \dfrac{x_2(k)|x_2(k)|}{2R} \end{cases} \tag{2.2.6}$$

where $sat(a,\delta) = \begin{cases} sign(a) & |a| > \delta \\ \dfrac{a}{\delta} & |a| < \delta \end{cases}$

The main limitation of (2.2.5) is the high frequency oscillation in the output signal. The problem is alleviated by using the approximation (2.2.6) but the quality of the differentiation suffers. This is because that the functions $-Rsign(x_1 - u + x_2|x_2|/2R)$ and $-Rsat(x_1 - u + x_2|x_2|/2R)$ both are solutions for the time optimal control problem for a continuous system instead of discrete system [18].

To improve the numerical properties and avoid high frequency oscillations the discrete form of NTD was derived directly in discrete time domain [1]:

$$\begin{cases} x_1(t+h) = x_1(t) + hx_2(t) \\ x_2(t+h) = x_2(t) + hfst_2(x_1(t), x_2(t), u(t), r, h_1) \end{cases} \tag{2.2.7}$$

where $u(t)$ is the input, h is the step size, h_1 is an additional parameter and the function $fst_2(x_1,x_2,u,r,h_1)$ is defined as:

$$\begin{aligned} & d = rh_1; \;\; d_0 = dh_1; \;\; y = x_1 - u + h_1 x_2; \\ & a_0 = \sqrt{d^2 + 8r|y|}; \;\; a = \begin{cases} x_2 + \dfrac{y}{h_1}, & |y| < d_0 \\ x_2 + \dfrac{sign(y)(a_0 - d)}{2}, & |y| \geq d_0 \end{cases}; \\ & fst_2 = \begin{cases} -r \;\; a/\;\delta & |a| \leq d \\ -r \;\; sign(a) & |a| > d \end{cases} \end{aligned} \tag{2.2.8}$$

It has been implemented as an s-function in Simulink.

A linear version of TD was given in [2] and is called LTD, which is defined:

$$\begin{cases} \dot{x}_1 = x_2 \\ \dot{x}_2 = -mR^2 x_1 - 2Rax_2 + mR^2 u(t) \end{cases} \tag{2.2.9}$$

where $x_1(t)$ and $x_2(t)$ are the states of the observer, *u(t)* is input signal, *m, a, R* are all positive parameters.

2.3 First-order Robust Exact Differentiator (RED)

In [3], the author believes the existing differentiators only provide approximate differentiation in the absence of noise. Thus, differentiation is robust but not exact, error does not decrease to zero in the presence of vanishing noise at any fixed time, and no asymptotic error analysis is sensible for any fixed differentiator parameter and time. So, he proposed the first-order robust exact differentiator (RED) via sliding mode technique.

The mathematical form of RED is:

$$\begin{cases} \dot{x}_1 = x_2 \\ x_2 = x_{21} - k\left|x_1 - u(t)\right|^{1/2} sign(x_1 - u(t)) \\ \dot{x}_{21} = -a\, sign(x_1 - u(t)) \end{cases} \tag{2.3.1}$$

where $x_2(t)$ is the output of the differentiator, *u(t)* is the input signal, and the sufficient condition for the convergence of $x_2(t)$ to $\dot{u}(t)$ was given in [3].

2.4 Observer-based Differentiators

To realize state feedback, it is necessary to measure the states of a system. But in some applications, some of the state variables may not be available at all, or it is not feasible to measure them. So, an *observer* is used to estimate state variables that are not accessible. Here, the observer is derived based on the model of the plant.

2.4.1 Linear State Observer (OBS)

Assume a system with transfer function

$$\frac{Y(s)}{U(s)}=\frac{b_m s^m+b_{m-1}s^{m-1}+\cdots+b_1 s+b_0}{s^n+a_{n-1}s^{n-1}+\cdots+a_1 s+a_0} \qquad m\le n \tag{2.4.1}$$

Its observable canonical form in state space is

$$\begin{cases}\dot{x}=Ax+Bu\\ y=Cx\end{cases} \tag{2.4.2}$$

where $A=\begin{bmatrix}0 & 1 & 0 & \cdots & 0\\ 0 & 0 & 1 & \cdots & 0\\ \vdots & \vdots & \vdots & & \vdots\\ 0 & 0 & 0 & \cdots & 1\\ -a_0 & -a_1 & -a_2 & \cdots & -a_{n-1}\end{bmatrix}$ $B=\begin{bmatrix}\beta_{n-1}\\ \beta_{n-2}\\ \vdots\\ \beta_1\\ \beta_0\end{bmatrix}$

$$C=\begin{bmatrix}1 & 0 & 0 & \cdots & 0\end{bmatrix}$$

where $\beta_n=b_n$

$$\beta_{n-1}=b_{n-1}-a_{n-1}\beta_n$$

$$\beta_{n-2}=b_{n-2}-a_{n-2}\beta_n-a_{n-1}\beta_{n-1}$$

$$\beta_0=b_0-\sum_{i=0}^{n-1}a_i\beta_{n-i}=b_0-a_0\beta_n-a_1\beta_{n-1}-\cdots-a_{n-1}\beta_1$$

Here, the state vector can be written as

$$x=\begin{bmatrix}y\\ \dot{y}\\ \ddot{y}\\ \vdots\\ y^{n-1}\end{bmatrix} \tag{2.4.3}$$

An observer of this system is:

$$\begin{cases} \dot{\hat{x}} = A\hat{x} + Bu + Le \\ \hat{y} = C\hat{x} \end{cases} \tag{2.4.4}$$

where $\hat{x}$ estimates the actual state vector x, $\hat{y}$ estimates the actual output vector y, $e = y - \hat{y}$, L is a constant gain vector, which can be determined using pole placement. Here, the estimated state vector $\hat{x}$ can be written as

$$\hat{x} = \begin{bmatrix} \hat{y} \\ \dot{\hat{y}} \\ \ddot{\hat{y}} \\ \vdots \\ \hat{y}^{(n-1)} \end{bmatrix} \tag{2.4.5}$$

The observer of a second-order system has two states. One of them can be used as the approximate differential signal.

Example 2.1

Using standard linear second-order system: $\frac{\omega_n^2}{s^2 + 2\xi\omega_n s + \omega_n^2}$ as the plant, whose state-space form is:

$$\begin{cases} \dot{x}_1 = x_2 \\ \dot{x}_2 = -\omega_n^2(x_1 - u(t)) - 2\xi\omega_n x_2 \\ y = x_1 \end{cases} \tag{2.4.6}$$

Suppose ξ=0.5, ω_n =200,

$$\begin{bmatrix} \dot{x}_1 \\ \dot{x}_2 \end{bmatrix} = \begin{bmatrix} 0 & 1 \\ -40000 & -200 \end{bmatrix} \begin{bmatrix} x_1 \\ x_2 \end{bmatrix} + \begin{bmatrix} 0 \\ 40000 \end{bmatrix} u$$
$$y = \begin{bmatrix} 1 & 0 \end{bmatrix} \begin{bmatrix} x_1 \\ x_2 \end{bmatrix} \tag{2.4.7}$$

The OBS of this system is:

$$\dot{\hat{x}} = A\hat{x} + Bu + Le \tag{2.4.8}$$

where $L = \begin{bmatrix} l_1 \\ l_2 \end{bmatrix}$

The characteristic polynomial of plant is:

$$s^2 + 2\xi\omega_n s + \omega_n{}^2 = s^2 + 200s + 4\times10^4 = 0 \tag{2.4.9}$$

The poles are: $s_{1,2} = \dfrac{-200 \pm \sqrt{4\times10^4 - 16\times10^4}}{2} = -100 \pm j50\sqrt{3}$

The characteristic polynomial of observer is:

$$\det\left|sI - (A - LC)\right| = \left\| \begin{bmatrix} s & 0 \\ 0 & s \end{bmatrix} - \begin{bmatrix} -l_1 & 1 \\ -4\times10^4 - l_2 & -200 \end{bmatrix} \right\|$$

$$= s^2 + (200 + l_1)s + 200l_1 + 40000 + l_2 \tag{2.4.10}$$

Suppose the desired observer poles are:

$$5s_{1,2} = -500 \pm j250\sqrt{3}$$

Then the desired observer characteristic polynomial is:

$$\left(s + 500 + j250\sqrt{3}\right)\left(s + 500 - j250\sqrt{3}\right) = s^2 + 1000s + 437500 \tag{2.4.11}$$

l_1=800 and l_2=2.375e5 can be solved by comparing the characteristic polynomial of observer with that of desired observer. Then they were applied in Simulink for tuning, consequently l_1=1, l_2=2.1x10^5.

2.4.2 Nonlinear State Observer (fal-obs)

To make the observer more sensitive to a small error and therefore achieving better performance, a nonlinear observer is proposed in [20]

$$\dot{\hat{x}} = A\hat{x} + Bu + Lfal(e) \tag{2.4.12}$$

where the *fal*-function is a nonlinear gain function shown in Figure 3. It has three parameters: x, α, δ and is defined as:

$$fal(x,\alpha,\delta) = \begin{cases} |x|^{\alpha} sign(x), & |x| > \delta, \\ \dfrac{x}{\delta^{1-\alpha}}, & |x| \le \delta, \end{cases} \qquad \delta > 0 \tag{2.4.13}$$

The graphical interpretation in Figure 3 shows the comparison of linear and nonlinear gains.

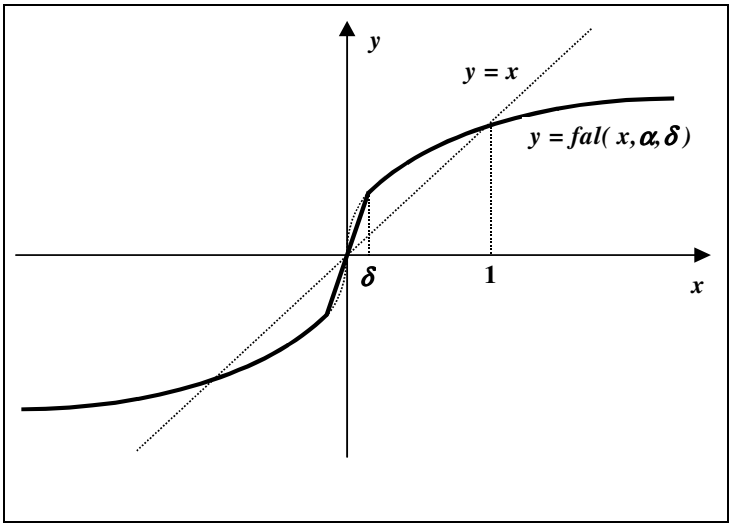

Figure 3 Comparison of linear and nonlinear gains

For here, let $x = e$. When α=1, *fal(e)* is equal to e. So the linear state observer can be considered as a special case of the nonlinear state observer.

2.4.3 Extended State Observer (ESO)

OBS and fal-obs both are model-based observers, but ESO is a model independent observer. Here we use an example to illustrate the concept of ESO [20].

A general second-order plant with unknown external disturbance can be described by

$$\ddot{y} = -a\dot{y} - by + w + bu \tag{2.4.14}$$

where y and u are output and input, respectively, and w is an unknown external disturbance. Both parameters, a and b, are unknown, although we have some knowledge of b, i.e. $b_0 \approx b$ (from, say, the initial acceleration of y in step response). Rewrite equation (2.4.14) as

$$\ddot{y} = -a\dot{y} - by + w + (b - b_0)u = f + b_0 u \tag{2.4.15}$$

Here $f = -a\dot{y} - by + w + (b - b_0)u$ is referenced as the generalized disturbance because it represents both the unknown internal dynamics, $-a\dot{y} - by + (b - b_0)u$ and the external disturbance w.

Rewrite the plant in (2.4.15) in state space form as:

$$\begin{cases} \dot{x}_1 = x_2 \\ \dot{x}_2 = x_3 + b_0 u(t) \\ \dot{x}_3 = h(t), \qquad h(t) = \dot{f}(t) \\ y = x_1 \end{cases} \tag{2.4.16}$$

where *h(t)* is the derivative of f and is unknown. The reason for increasing the order of the plant is to make f a state so that a state observer can be used to estimate it. One such observer is given as

$$\begin{cases} \dot{z}_1 = z_2 - \beta_{01} fal(e, \alpha_1, d_1) \\ \dot{z}_2 = z_3 - \beta_{02} fal(e, \alpha_2, d_2) + b_0 u \\ \dot{z}_3 = -\beta_{03} fal(e, \alpha_3, d_3) \end{cases} \tag{2.4.17}$$

where $\beta_{01}, \beta_{02}, \beta_{03}$ are observer gains, and b_0 is the normal value of b. This observer is denoted as the extended state observer (ESO). With the gains properly selected, the observer will track the states and yield

$$z_1(t) \to y(t),\ z_2(t) \to \dot{y}(t),\ z_3(t) \to f(t, y, \dot{y}, u, w) \tag{2.4.18}$$

When b_0=0, $z_3(t) \to \ddot{y}(t)$

CHAPTER III

COMPARATIVE STUDY OF DIFFERENTIATION TECHNIQUES

In this chapter, first, each differentiator is explored in time domain and frequency domain to establish the relationship between design parameters and performance. This helps the user to gain insights on how these differentiators work via responses in time domain and analysis in frequency domain. Then various differentiators are compared in terms of their responses for a standard second order system's output and a given measurement noise level. Finally, different double differentiators are compared.

3.1 Differentiator Response in Time Domain and Analysis in Frequency Domain

Time domain response and frequency domain analysis are basic evaluation tools in classical control theory. The characteristics of the following differentiators are derived via these two methods.

3.1.1 Classical Linear Approximation Differentiators

There are two forms of LADs. They are separately described using equation (2.1.2) and equation (2.1.9). Equation (2.1.9) can be rewritten as

$$\frac{1}{\tau_2-\tau_1}\cdot\frac{(\tau_2-\tau_1)s}{(\tau_1 s+1)(\tau_2 s+1)}=\frac{s}{(\tau_1 s+1)(\tau_2 s+1)} \tag{3.1.1}$$

It is a second-order system. Comparing equation (3.1.1) and equation (2.1.2) when m=2, the simulation block diagram was set up in Figure 4. The choice of three parameters τ, τ_1, τ_2 was listed in Table 1 with $\tau^2=\tau_1\times\tau_2$. The responses are shown in Figure 5.

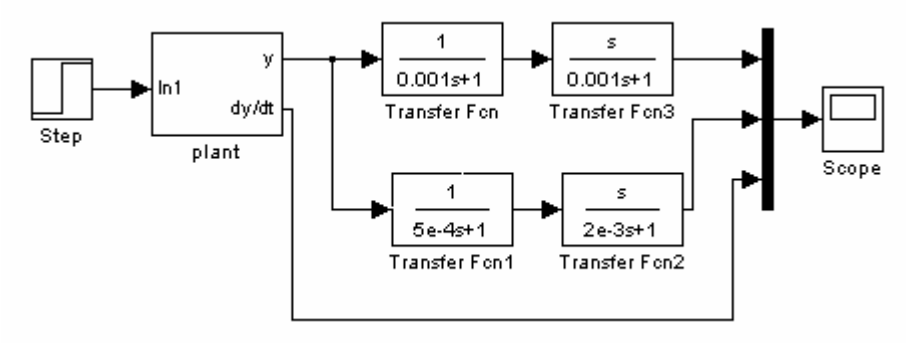

Figure 4. The block diagram for two kinds of second-order classical differentiators

Table 1. Three sets of parameters for two kinds of second-order classical differentiators

		Set 1	Set 2	Set 3
Same τ	τ	10^{-3} Poles = -1000, -1000		
Different τ	τ_1	10^{-5}	10^{-4}	$5\text{x}10^{-4}$
	τ_2	0.1	10^{-2}	$2\text{x}10^{-3}$
		Poles = -10^5, -10	Poles = -10^4, -10^2	Poles = -2000, -500

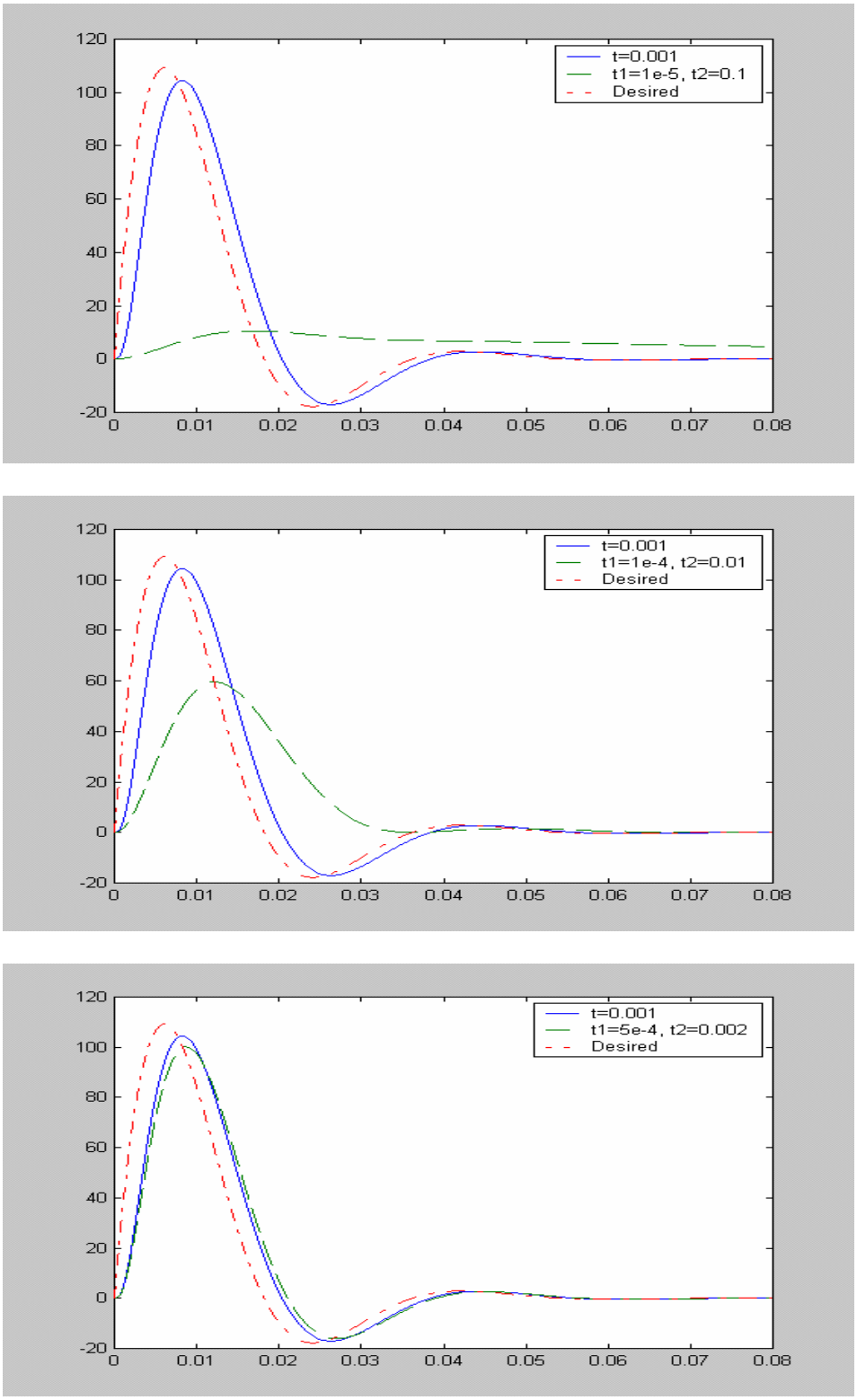

Figure 5. Comparing results for two kinds of second-order classical differentiators for different parameters

From Table 1 and Figure 5, it is clear that the closer the τ_1 and τ_2 the better the performance. When $\tau_1 = \tau_2 = \tau$, the differentiator generates the best differential signal. Therefore, we set $\tau_1 = \tau_2$ for all simulation from this point on. That is, only equation (2.1.2) is used as the linear approximation differentiator.

Next, we evaluate the performance of (2.1.2) for different orders. Step responses of different order classical linear approximation differentiators are used to evaluate in the time domain. The block diagram was set up in Figure 6. The responses are shown in Figure 7.

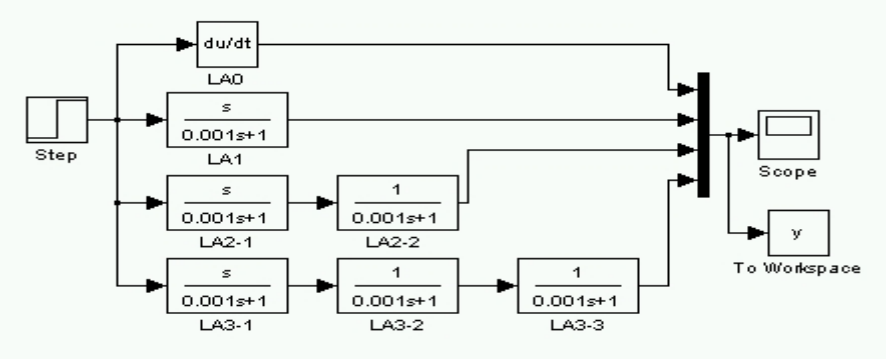

Figure 6. The block diagram for classical differentiators

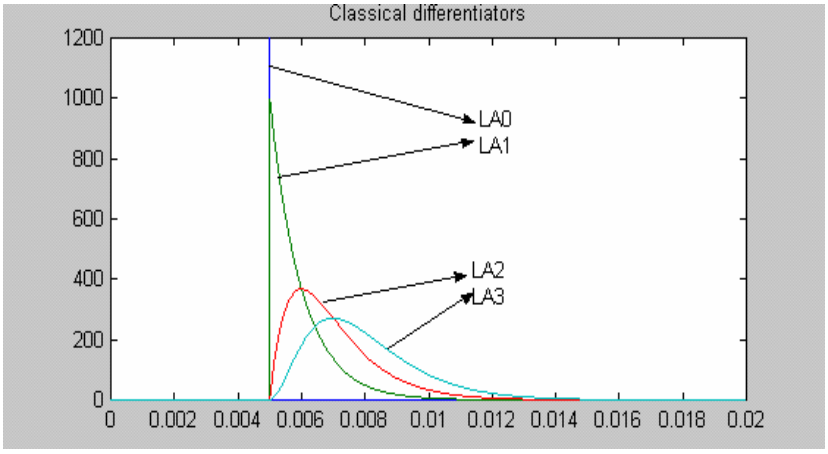

Figure 7. The step responses of LA differentiators under different order m

(m=0,1,2,3; τ=0.001)

The step response of the differentiator should be an impulse. So, Figure 7 indicates that as *m* gets bigger, the performance of approximated differentiator becomes worse.

The frequency responses of different order LAD are shown below.

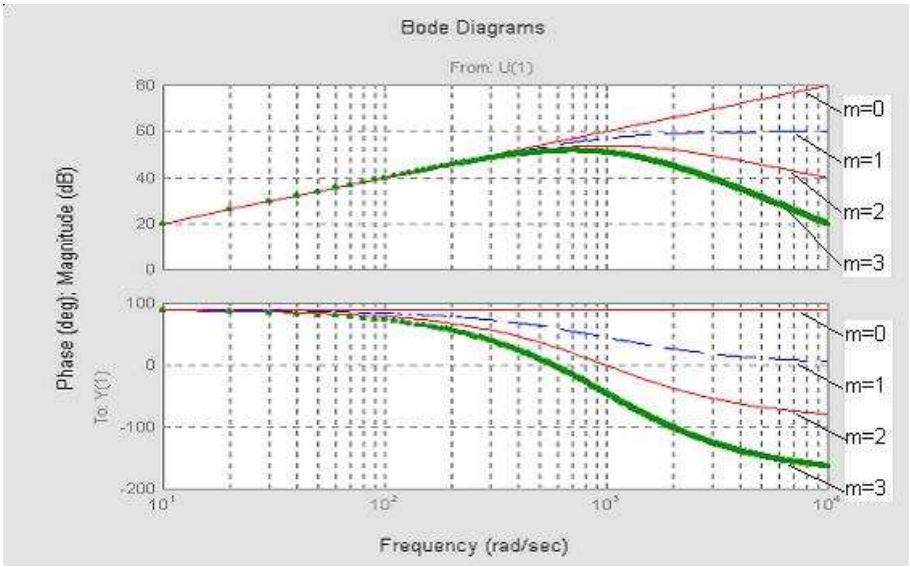

Figure 8. The frequency response of LAD under different order m

(*m*=0,1,2,3; from top to bottom, τ=0.001)

It can be seen that as *m* gets bigger, the more attenuation at high frequency.

From the response in time domain and analysis in frequency-domain, we can see that there is a tradeoff between accuracy and noise sensitivity. This is reflected in the selection of *m*.

3.1.2 Nonlinear Tracking Differentiator

The NTD described in equation (2.2.7) is first evaluated in the time domain for different *R,* where *R* represents the maximum acceleration the system can attain. It is the

only design parameter for NTD. The step responses of NTD are shown in Figure 9. As *R* varies from 20 to 2000, the response becomes faster.

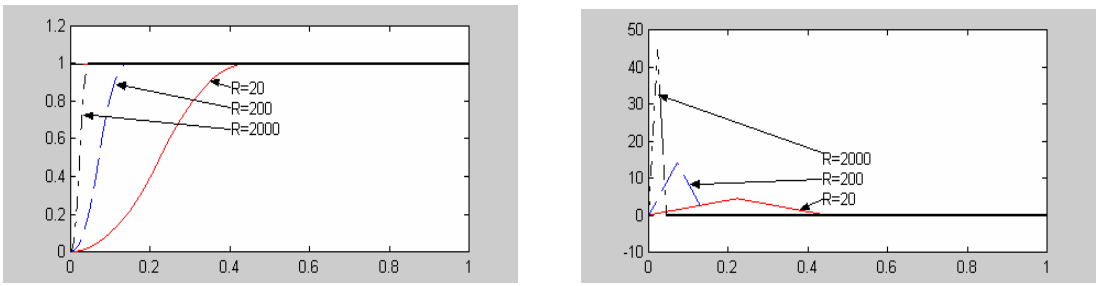

Responses of $x_1(t)$ Responses of $x_2(t)$

Figure 9. The step responses of $x_1(t)$ and $x_2(t)$ of NTD under different *R* (*R*=20, 200, 2000, from right to left)

The responses of $x_1(t)$ under different *R* never overshoot the target, which means that $x_1(t)$ can track *u(t)* no matter how fast it is, but never overshoots the target. In particular, $x_1(t)$ converges to *u(t)* in the shortest time possible under the constraint that the rate of change for $x_2(t)$, or the acceleration of $x_1(t)$, is bounded by *R*. In other words, the NTD "blocks" any part of the signal with the acceleration greater than *R*.

Figure 10 and Figure 11 show the frequency responses of the NTD. They were obtained by feeding NTD a sinusoidal input, $u(t)=A\sin(\omega t)$, of various ω and measure the magnitude and phase change in the output. The magnitude and phase plots are shown for different *R* and the input amplitude *A*.

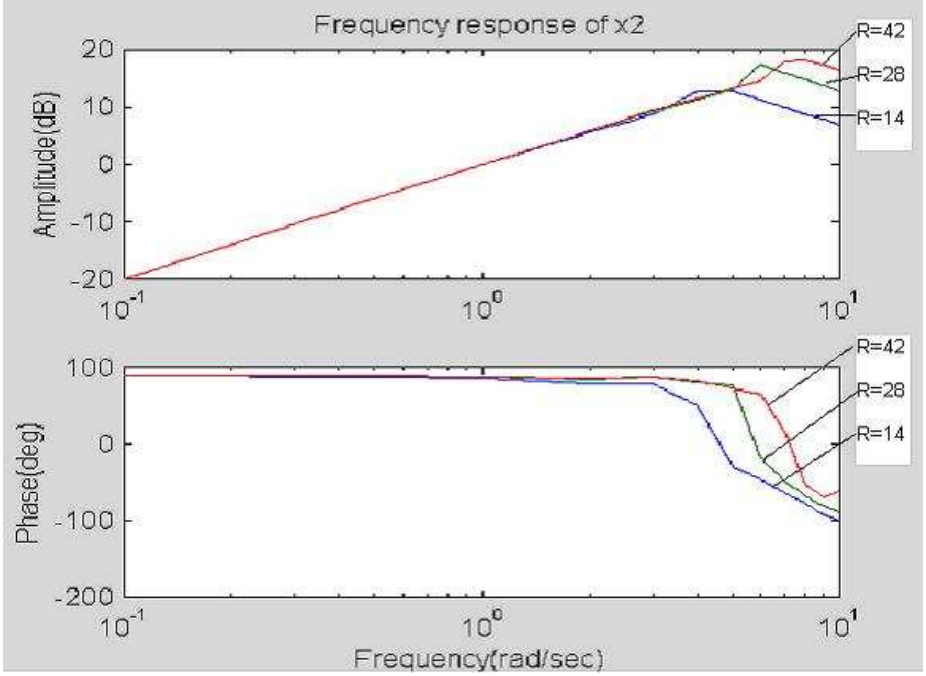

Figure 10. The frequency response of $x_2(t)$ of NTD when $u(t)=\sin(\omega t)$, R=14,28,42

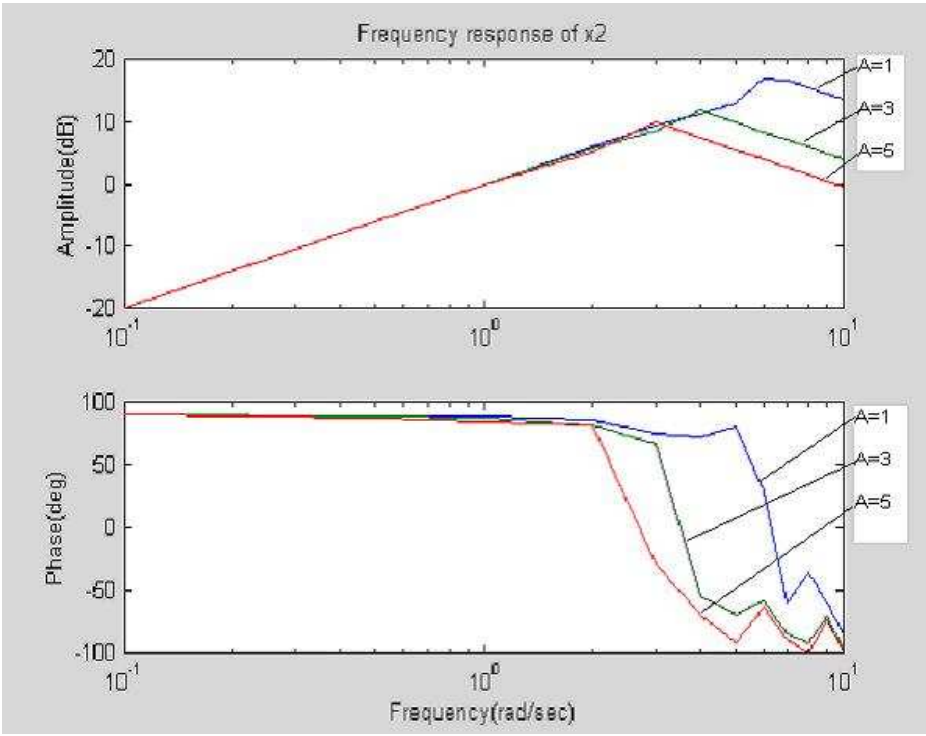

Figure 11. The frequency response of $x_2(t)$ of NTD when $u(t)=A\sin(\omega t)$, R=30, A=1,3,5

It is very easy to see the frequency response properties of NTD and their relationship to *R* and the amplitude *A* of the input signal.

The frequency response corresponding to the second output signal $x_2(t)$ has a +20dB/sec slope in the magnitude plot and +90 degrees in the phase plot at corner frequency. As the frequency passes the critical point corresponding to the peak in the magnitude, there is a sudden switch of slope and its amounts to a change of –40dB. This quick change in slope ensures a much better noise rejection property.

The impact of NTD is profound. As a noise filter, it blocks any part of the signal with acceleration rates exceeding *R*. In practice, we often know the physical boundary of a signal in terms of its acceleration rate. This knowledge can be conveniently incorporated into NTD to reject noise based on the understanding of the physics of the plant. On the other hand, the traditional linear filter can only attenuate noises based on its frequency contents.

The most important role of NTD is its ability to obtain the derivative of a noisy signal with a good signal to noise ratio. It is well known that a pure differentiator is not physically possible to implement. The error is often not differentiable in practice due to the noise in the feedback and the discontinuities in the reference signal. This explains why the PID controller is used primarily as a PI controller in most applications. The use of the "D" part has been quite limited due to the extreme amplification of noise by differentiation, or its approximations. This noise problem is resolved in NTD because x_2 is obtained via integration. This idea of using integration to obtain differentiation goes back to 1920s when N. Wiener proposed the definition of "fractional differentiation" based

on integration. It leads to the concepts of generalized function and generalized derivative, which were used widely in the theory of partial differential equations.

3.1.3 Linear Tracking Differentiator (LTD)

The LTD described in equation (2.2.9) has three parameters. When m=2, a=1, R=10, 100, 1000, the step responses of two states are shown below:

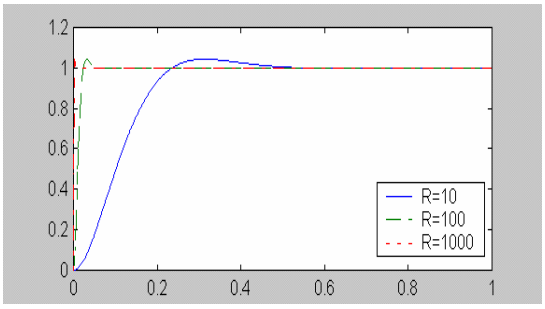

Responses of $x_1(t)$

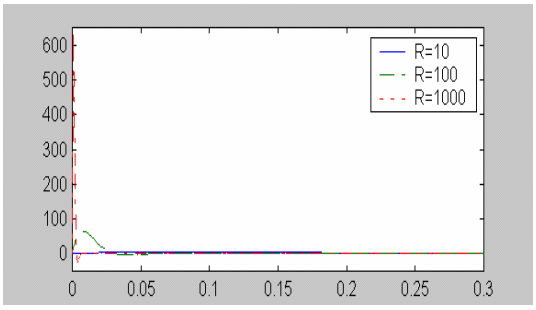

Responses of $x_2(t)$

Figure 12. The step responses of $x_1(t)$ and $x_2(t)$ of LTD under different R

As R varies from 10 to 1000, the responses become faster, but they have overshoot. So, the LTD is not as good as NTD.

3.1.4 First-order Robust Exact Differentiator (RED)

The RED described in equation (2.3.1) has two parameters a and k. When k=6, a=8, 80, 800 and a=8, k=6, 60, 600, the step responses of two states are shown in Figure 13.

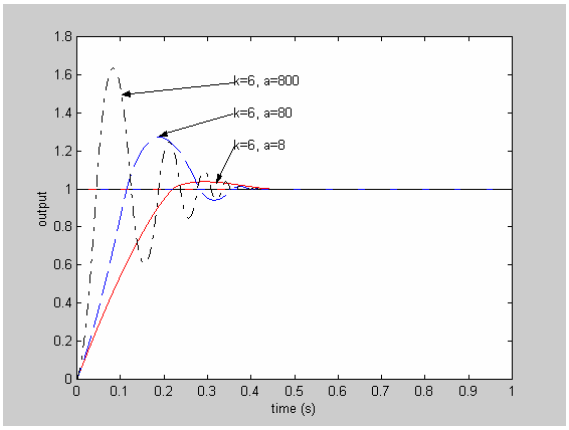

Responses of $x_1(t)$

with same *k* and different *a*

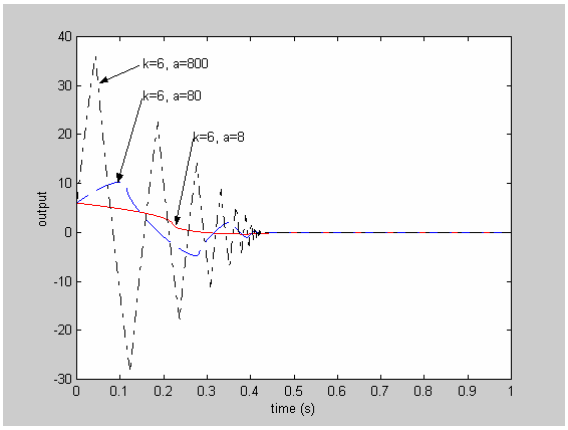

Responses of $x_2(t)$

with same *k* and different *a*

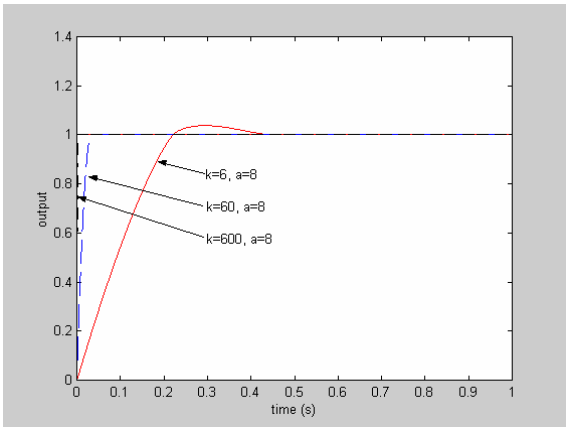

Responses of $x_1(t)$

with different *k* and same *a*

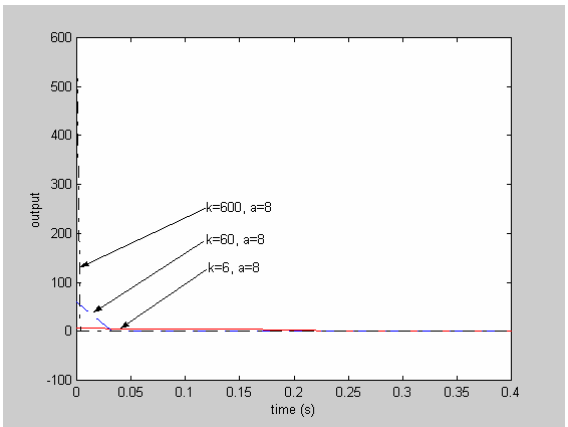

Responses of $x_2(t)$

with different *k* and same *a*

Figure 13. The step responses of the RED under different parameters

Figure 13 shows the parameters of RED, when *k* is fixed, the responses become faster as *a* varies from 8 to 800, but they have overshoot and oscillation whatever the responses of $x_1(t)$ or $x_2(t)$. When *a* is fixed, the responses become faster as *k* varies from 6 to 600

and the overshoot of the response of $x_1(t)$ is blocked, the differential signal $x_2(t)$ is much better.

3.2 Time Domain Comparison

In this section, we will determine which one is the best differentiation method, for this purpose. First, the NTD, RED, LA1 and LA2 are compared in continuous time domain. Then the NTD and LA2 are compared in discrete time domain. Finally, the OBS, fal-obs with NTD and LA2 are compared in discrete time domain.

3.2.1 Simulation Setup and Comparison in Continuous Time Domain

The simulation block of the plant to be used is shown in Figure 14, which has a standard second-order system: $\frac{\omega_n^2}{s^2 + 2\xi\omega_n s + \omega_n^2}$. There are two outputs for the block diagram of the plant. One is the real output *y(t)*, the other is the differential signal of the real output, *dy/dt*. NTD, RED, LA1 and LA2 are compared together. The output *y(t)* of the plant is the input of differentiators. There are two outputs for every differentiator except LA1. The first output tracks *y(t)*. The second output tracks *dy/dt*. We will determine which differentiator tracks *dy/dt* closer, and which one has better differential performance. The comparing diagram is:

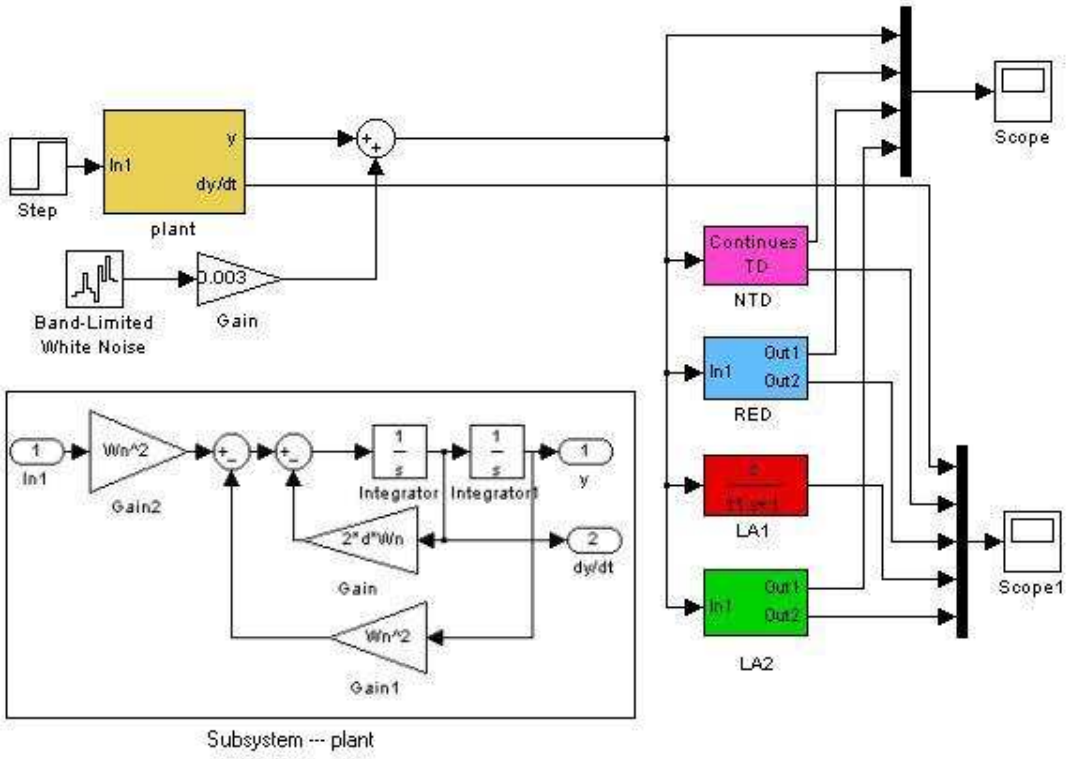

Figure 14. Comparing differentiators

First, we make these differentiators track the plant's differential signal as close as possible. The parameters of various differentiators are tuned. They are listed below:

Plant: ξ=0.5; ω_n=200; NTD: R=10^7;h=10^{-4}; RED: a=35;k=60;

LA1: τ_1=10^{-4}; LA2: τ_2=10^{-4};

Simulating results are shown in Figure 15. Every differentiator except RED has good tracking properties.

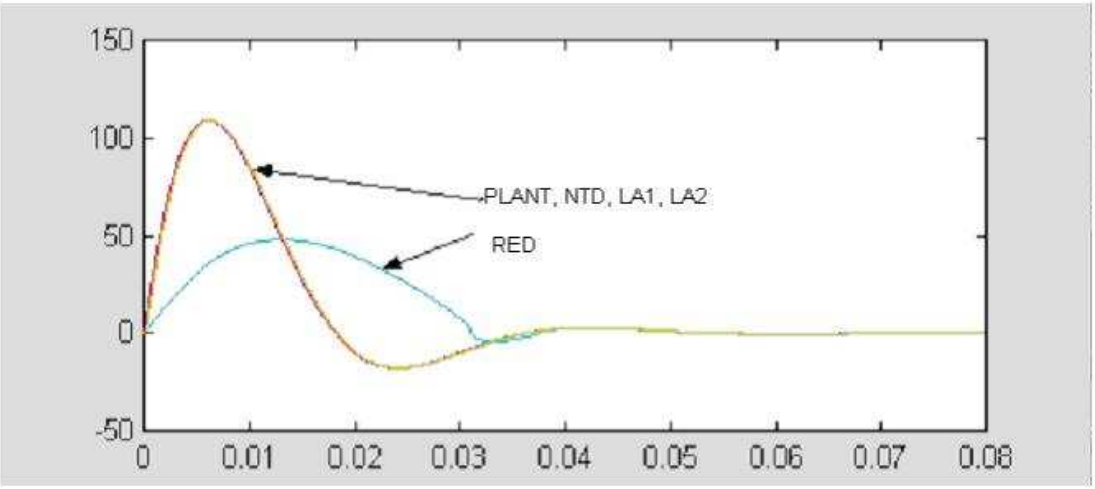

Figure15. Comparison result of differentiators

Next, to make the comparison fair, white noise (10%) was supplied to the differentiators and the parameters were adjusted so that the differentiators yield the same level of noise amplification. The retuned parameters are:

Plant: ξ=0.5; ω_n=200; NTD: R=10^7; h=0.001; RED: a=18;k=15;

LA1: τ_1=0.03; LA2: τ_2=0.001;

The simulation results are shown in Figure 16. The NTD and the LA2 have very similar performances, which are the best among all the differentiators. The LA1 and the RED did not perform very well [4].

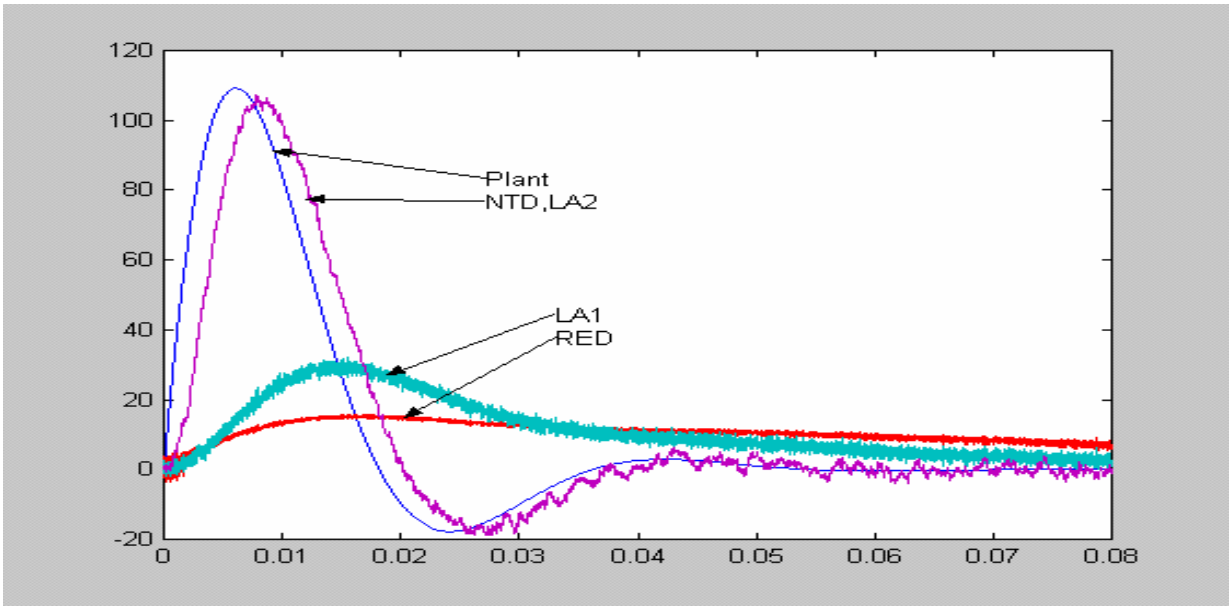

Figure 16. Comparison result of differentiators with white noise

3.2.2 Comparison of the NTD and LA2 in Discrete Time Domain

The NTD and LA2 were compared in discrete time domain by using the same method as in section 3.2.1, i.e., white noise (10%) was supplied to these two differentiators and the parameters were adjusted so that they yield the same level of noise amplification. Then their performance was compared. The new parameters are: R=10^6, h=0.0011, τ_2 =0.001. The sampling time T=0.1ms. The results are shown below:

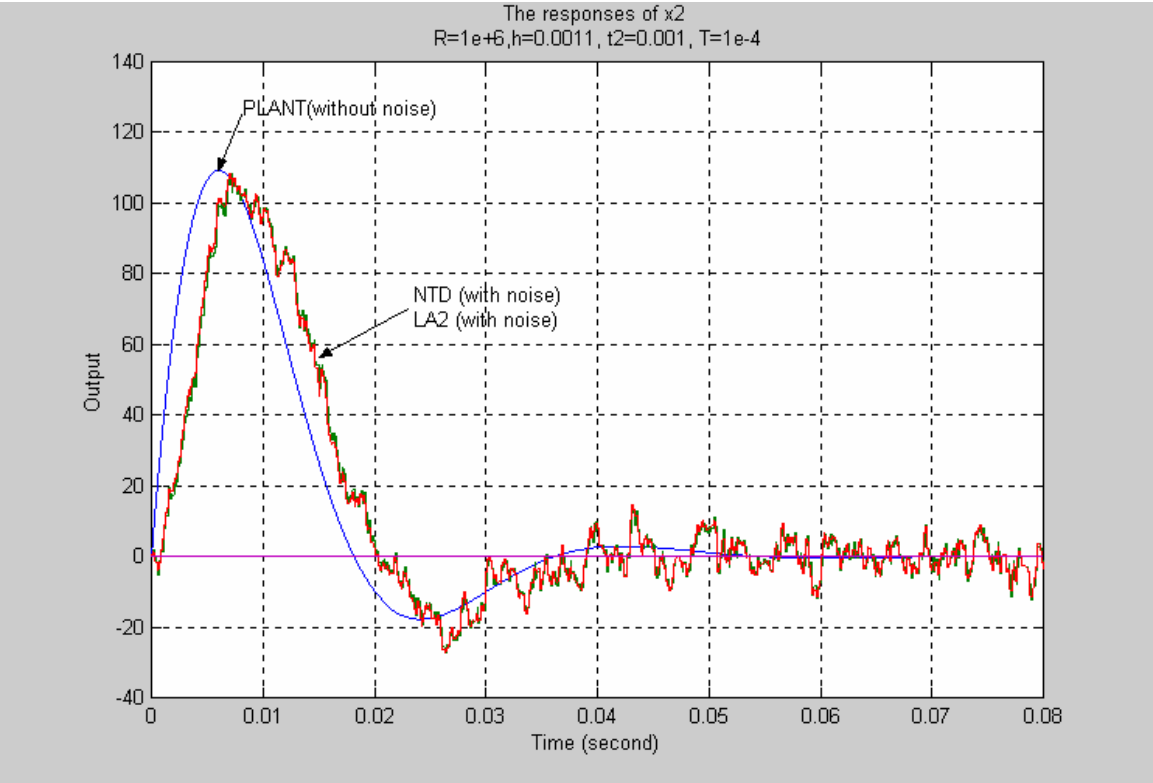

Figure 17. Comparison of the responses NTD and LA2 in discrete time domain

It is hard to tell which one is better from Figure 17. So the Correlation Coefficient was used to evaluate the responses [10]. In general, correlation is an analysis technique that is used to determine how similar two signals are. In signal processing, correlation is typically used to evaluate the relationship of the value of a signal one time to those at previous times. In systems analysis, correlation techniques are often used to evaluate relationships between two signals across time, which is of particular interest in the study of dynamic system. In other words, correlation analysis techniques are used to evaluate the temporal structure of a signal or the temporal relationships between two different signals. The correlation coefficient, in general, indicates similarity between signals. The mathematical form is:

$$\frac{\sum xy - \frac{\sum x \sum y}{n}}{\sqrt{\left(\sum x^2 - \frac{(\sum x)^2}{n}\right)\left(\sum y^2 - \frac{(\sum y)^2}{n}\right)}} \tag{3.1}$$

The closer the Correlation Coefficient to 1, the more similar the two signals. Table 2 shows the relationship of the responses of NTD, LA2 and the original plant differential signal separately.

Table 2 Comparison of the responses NTD and LA2 in discrete time domain

	NTD	LA2
Correlation coefficient	0.9111	0.9203

It is obvious that LA2 is better than NTD.

3.2.3 Comparing OBS, fal-obs with NTD and LA2

The OBS and fal-obs methods were compared with NTD and LA2 by using the same method as in section 3.2.1, i.e., white noise (10%) was supplied to these systems and the parameters were adjusted so that they yield the same level of noise amplification. Then the performance of the differentiators were compared. The parameters are:

Table 3. The parameters of four kinds of differentiators

NTD	R=10^6, h=0.0011	
LA2	τ_2 =10^{-3}	
OBS	l_1=1	l_2=2.1x10^5
fal-obs	0.05, 0.01, 1	1.5, 0.01, 1.1x10^6
	0.05, 0.01, 1	0.5, 0.01, 40400

The responses of differentiators are shown in Figure18.

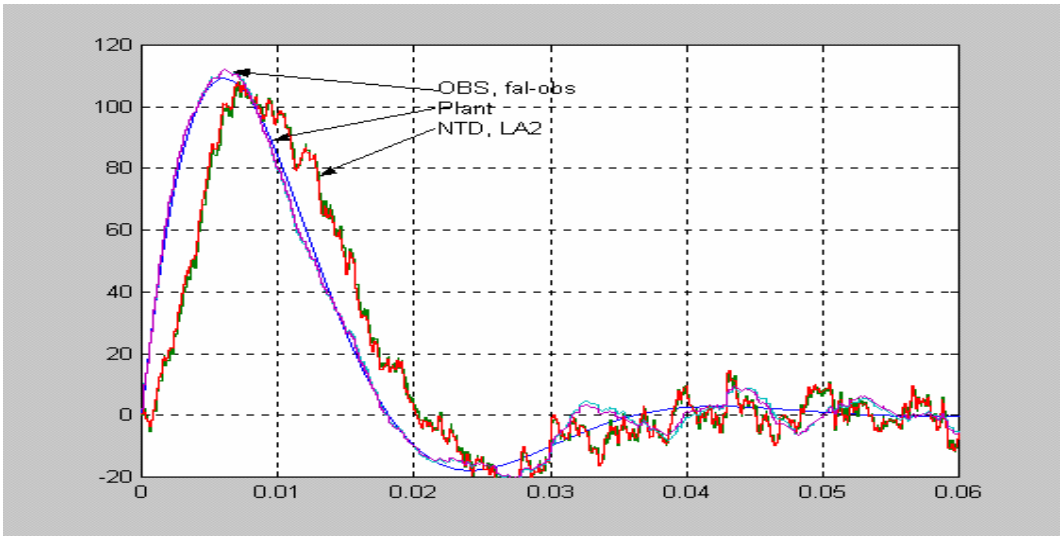

Figure 18. The responses of OBS, fal-obs, NTD and LA2

We can see clearly from Figure 18 that the output signals from NTD and LA2 are much more noisy than those from OBS and fal-obs. Then, separately, OBS and fal-obs were compared.

When α>1, the comparing plots are shown in Figure 19.

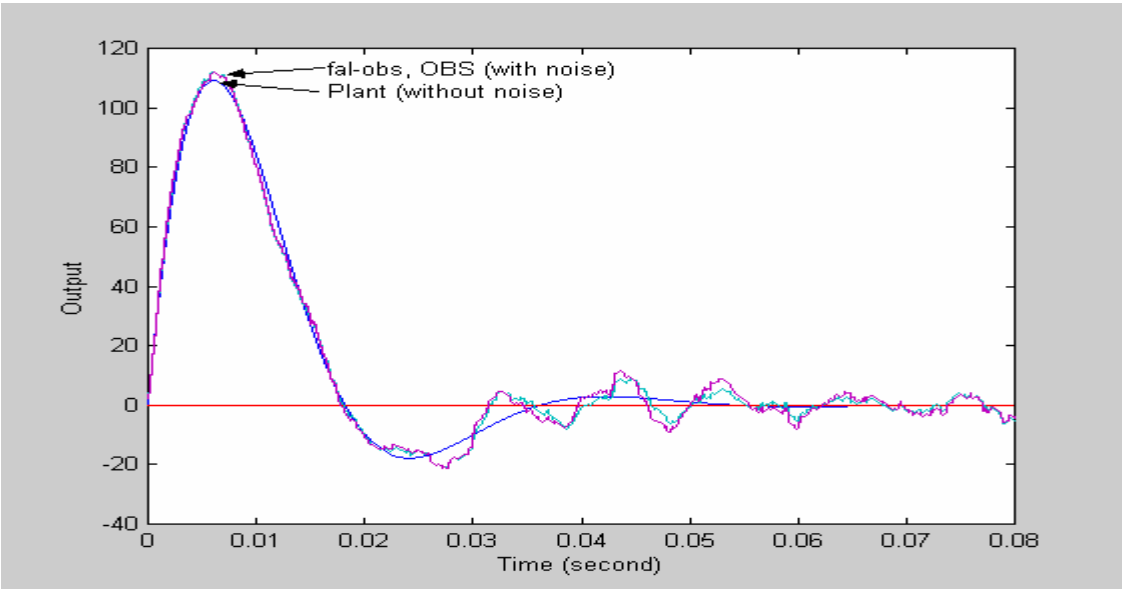

Figure 19. The responses of OBS and fal-obs when α>1

It is hard to tell which one is better from Figure 19. Again, the Correlation Coefficient was used to evaluate the responses.

Table 4. The responses of OBS and fal-obs when α>1

	OBS	fal-obs
Correlation coefficient	0.9944	0.9997

They are very close. The fal-obs is a little bit better than OBS in this case.

When α<1, the comparing plot is shown in Figure 20.

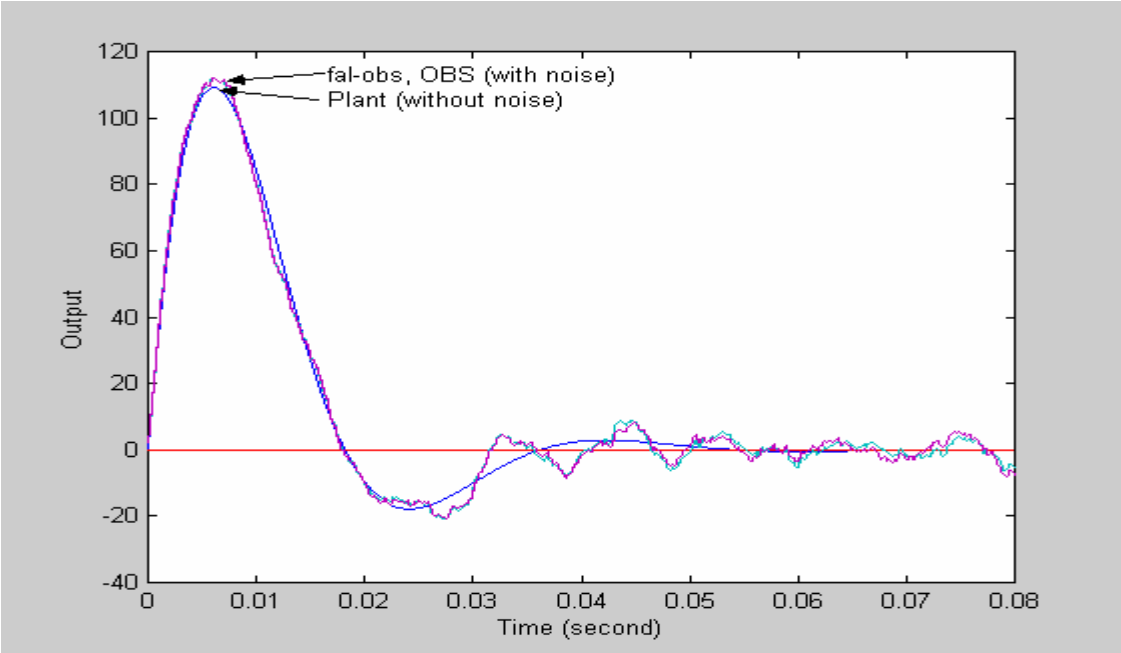

Figure 20. The responses of OBS and fal-obs when α<1

Using Correlation Coefficient to evaluate the responses.

Table 5. The responses of OBS and fal-obs when α<1

	OBS	fal-obs
Correlation Coefficient	0.9944	0.9945

They are very close. The fal-obs is a little bit better than OBS in this case, too.

So, using linear and nonlinear state observer (OBS and fal-obs) both can get the best differential signals. But these observers have their limitation. They depend on the plant. Therefore, when the plant is changed it is better to choose LA2 to get a differential signal.

3.3 Comparison of double differentiators

In this section, LA2 and LA2, NTD and NTD, LA2 and LA1 are cascaded respectively, thus they can generate double differential signals, x_3 ($x_3 = \ddot{x}_1$). OBS and fal-obs can not be cascaded because they are model-dependent. By using the same method as in the section before, the responses of x_3 ($x_3 = \ddot{x}_1$) of LA2-LA2, NTD-NTD, LA2-LA1 and ESO are compared. The new parameters are:

LA2-LA2: τ=0.001; τ_2=0.001;

NTD-NTD: R_1=10^6; h_1=0.0011; R_2=7x10^6; h_2=0.001;

LA2-LA1: τ=0.001; τ_1=0.003;

ESO: 6000ω, 1, 0.001; 1.7x$10^6\omega^2$, 0.5, 0.001; 9x$10^8\omega^3$, 0.25, 0.001;

0, 0, 0,10^{-4};

ω=0.3

The comparing diagram is shown in Figure 21.

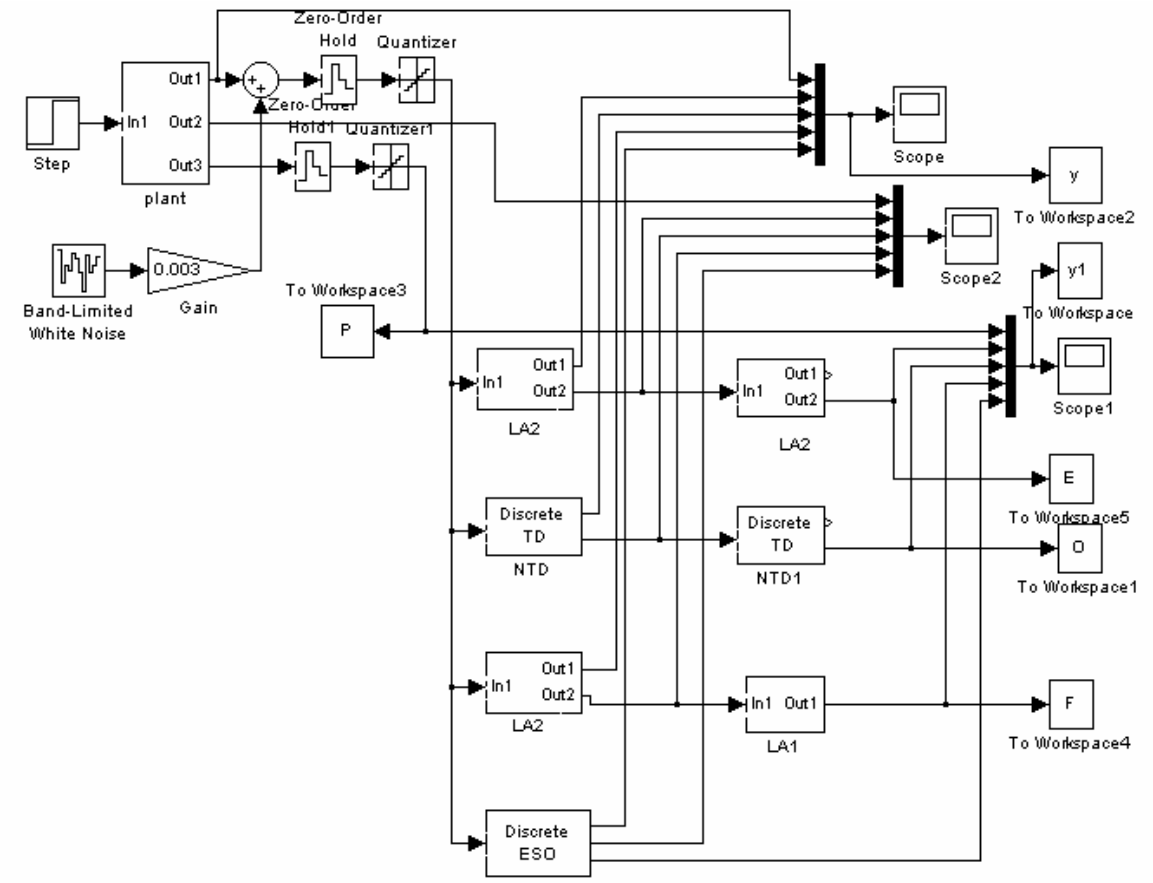

Figure 21. Comparison of double differentiators

The results are shown in Figure 22.

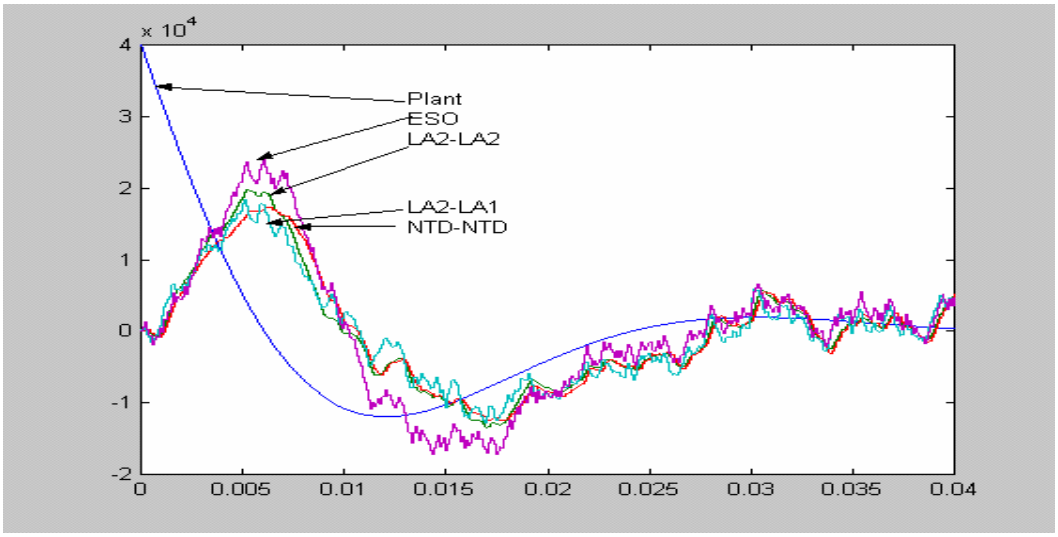

Figure 22. The responses of double differentiators

Using correlation coefficient to evaluate the responses.

Table 6 The responses of double differentiators

	LA2-LA2	LA2-LA1	NTD-NTD	ESO
Correlation coefficient	0.3760	0.3298	0.3094	0.3847

It can be concluded that ESO provides the best approximation of $\ddot{u}(t)$, then followed by LA2-LA2, LA2-LA1 and NTD-NTD.

CHAPTER IV

COMPARATIVE STUDY OF INTEGRATION TECHNIQUES

In this chapter, the linear integrator, the Clegg integrator, the nonlinear integrator and modified nonlinear integrator are described. Then they are analyzed using a describing function and compared according to their describing functions. Finally, they are compared in the PWM DC-DC power converter system.

4.1 Description of Four Kinds of Integrators

The linear integrator, the Clegg integrator, the nonlinear integrator and modified nonlinear integrator are described below.

4.1.1 Linear Integrator

The Linear integrator has an input *x(t)* and an output *y(t)* obeying the relationship

$$y(t) = y(0) + \int_0^t x(\tau) d\tau \tag{4.1.1}$$

where τ is the dummy variable of integration. By setting y(0)=0 and transforming the equation, the transfer function of the linear integrator can be derived as Y(s)/X(s)=1/s.

4.1.2 The Clegg Integrator

The Clegg Integrator is an integrator that resets to zero whenever its input crosses zero, and is an ordinary integrator between zero crossings. Its describing function is [17]:

$$D(j\omega) = \frac{1.62e^{-j38.1^\circ}}{\omega} \tag{4.1.2}$$

It has the same magnitude characteristic as a linear integrator of gain 1.62, but its phase lag at all frequencies is -38.1°.

4.1.3 Nonlinear Integrator

The main purpose for using integral control part is to eliminate the steady state error. Setting the integral gain too high can cause overshoot, wind-up, etc. A mathematical description of an integrator is shown in equation (4.1.3). This is denoted as the nonlinear integrator. The corresponding G-function for the nonlinear integrator is shown in Figure 23. The integrator is allowed to integrate only when the error is "small", typically when the output is within 10% of the set point. This design strategy allows the control to effectively avoid undesirable overshoots and integrator wind-up during transients.

$$\text{y} = \int g_i(e)dt \tag{4.1.3}$$

where $g_i(e) = \begin{cases} 0, & |e| > \delta \\ ke, & |e| \le \delta \end{cases}$ $\delta > 0$,

and k is the slope of G-function.

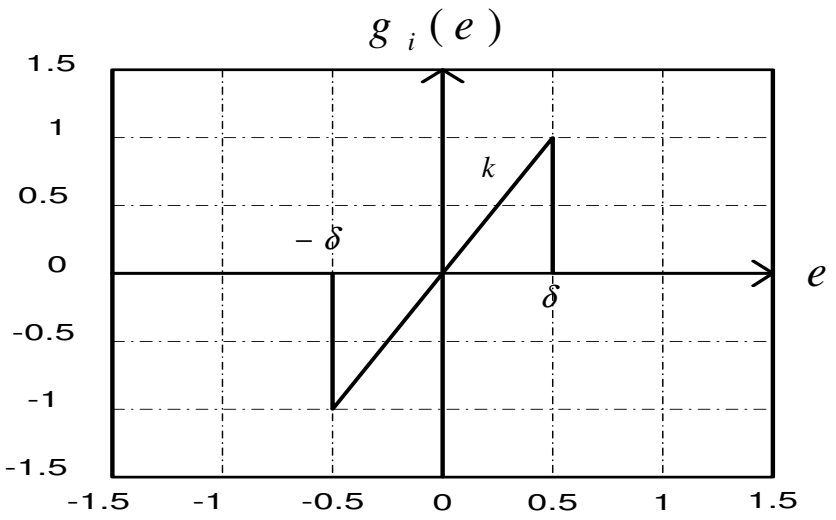

Figure 23. G-function for nonlinear integrator

4.1.4 Modified Nonlinear Integrator

This modification was based on the Clegg and the nonlinear integrators that were described before. This integrator resets to zero whenever its input crosses zero, and is a nonlinear integrator between zero crossings. Its mathematical form is:

$$y=\begin{cases}\int g_i(e)dt & e \neq 0 \\ 0 & e = 0\end{cases} \tag{4.1.4}$$

where $g_i(e)=\begin{cases}0, & |e|>\delta \\ ke, & |e|\le\delta\end{cases}$ $\delta>0$,

4.2 Integrator Analysis Using a Describing Function

The describing function is a common tool for the analysis of nonlinear dynamic system. It is obtained by applying a sinusoidal signal $a\sin\omega t$ at the input of the nonlinearity and calculating the ratio of the first harmonic at the output to *a.*

4.2.1 The Clegg Integrator

The response of the Clegg Integrator to a sinusoidal input is shown in Figure 24.

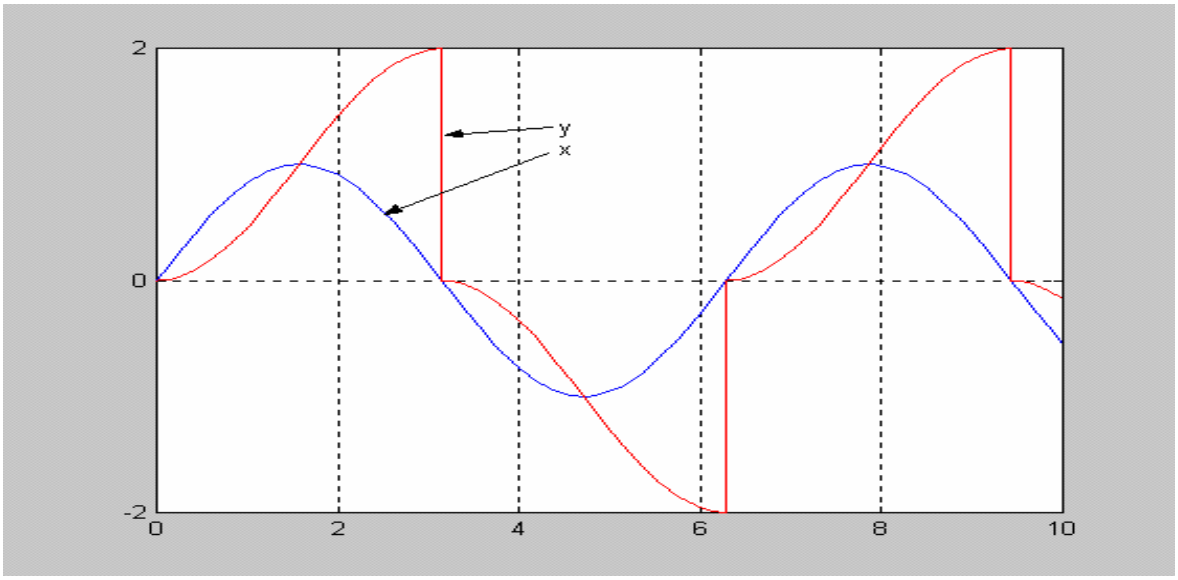

Figure 24. Sinusoidal response of Clegg Integrator

The block diagram is shown below

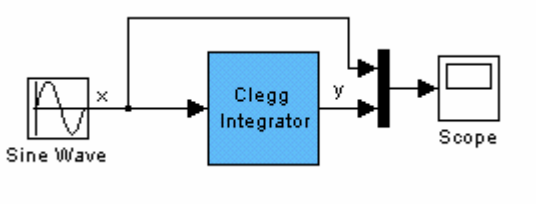

The general expression of the describing function is:

$$D(j\omega)=y(j\omega)/x(j\omega) \tag{4.2.1}$$

where y(jω) is output and x(jω) is input. Let x=Asin(ωt), from Figure 24, then

$$y=\int_0^t x(t)dt=\int_0^t A\sin(\omega t)dt=\frac{A}{\omega}(1-\cos(\omega t)) \tag{4.2.2}$$

Using equation (4.2.2) in the derivation (i.e. Fourier's series expansion) of the describing function

$$D(A, \omega)=[b_1(\omega)+j\, a_1(\omega)]/A \qquad (4.2.3)$$

where $a_1(\omega)=\frac{2}{\pi}\int_0^{\pi} x(\phi)\cos\phi d\phi=\frac{2}{\pi}\int_0^{\pi}\frac{A}{\omega}(1-\cos\phi)\cos\phi d\phi$

$$=\frac{2A}{\pi\omega}\left(\int_0^{\pi}\cos\phi d\phi-\int_0^{\pi}(\cos\phi)^2 d\phi\right)$$

$$=-\frac{2A}{\pi\omega}\left(0+\frac{\pi}{2}\right)=-\frac{A}{\omega}$$

$b_1(\omega)=\frac{2}{\pi}\int_0^{\pi} x(\phi)\sin\phi d\phi=\frac{2}{\pi}\int_0^{\pi}\frac{A}{\omega}(1-\cos\phi)\sin\phi d\phi$

$$=\frac{2A}{\pi\omega}\left(\int_0^{\pi}\sin\phi d\phi-\int_0^{\pi}\cos\phi\sin\phi d\phi\right)$$

$$=\frac{2A}{\pi\omega}(2+0)=\frac{4A}{\pi\omega}$$

So, $D(A,\omega)=\left(\frac{4A}{\pi\omega}-j\frac{A}{\omega}\right)/A=\frac{4}{\pi\omega}-j\frac{1}{\omega}$

$$=\frac{1}{\omega}\sqrt{\left(\frac{4}{\pi}\right)^2+1}\ \angle\ arctg\frac{-\pi}{4}$$

$$=\frac{1.62}{\omega}\ \angle\ -38.1^{\circ} \qquad (4.2.4)$$

It has the same magnitude characteristic as a linear integrator of gain 1.62, but its phase lag at all frequency is -38.1°.

4.2.2 Nonlinear Integrator

The response of the nonlinear integrator to a sinusoidal input is shown below:

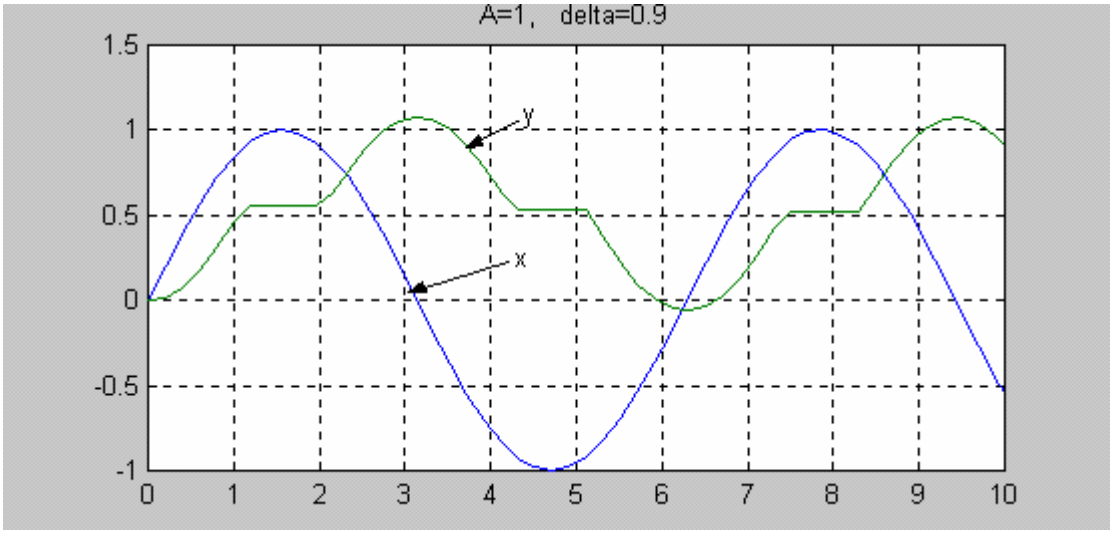

Figure 25. Sinusoidal response of Nonlinear Integrator when A=1, δ=0.9

For the nonlinear integrator, if the input signal $x = A\sin\theta$, $\theta = \omega t$, the output of G-function is

$$z = \begin{cases} 0 & |x| > \delta \\ kx & |x| \le \delta \end{cases} \qquad \delta > 0 \tag{4.2.5}$$

If $x = \delta$, then $A\sin\theta = \delta \Rightarrow \theta = \arcsin\dfrac{\delta}{A}$, thus

$$\mathrm{z} = \begin{cases} 0, & |\theta| > \arcsin\dfrac{\delta}{A} \\ kA\sin\theta, & |\theta| \le \arcsin\dfrac{\delta}{A} \end{cases} \qquad \delta > 0 \tag{4.2.6}$$

So, when $|\theta| \le \arcsin\dfrac{\delta}{A}$, the output of integrator will be

$$y = \int_0^t kA\sin(\omega t)dt = \frac{kA}{\omega}\left(1 - \cos(\omega t)\right) \tag{4.2.7}$$

The describing function is D(A, ω)=[$b_1(\omega)$+j $a_1(\omega)$]/A

where $a_1(\omega)=\frac{1}{\pi}\int_0^{2\pi} y(\phi)\cos\phi d\phi$

$$=\frac{1}{\pi}\left[\int_0^{\arcsin\frac{\delta}{A}}\frac{kA}{\omega}(1-\cos\phi)\cos\phi d\phi+\int_{\pi-\arcsin\frac{\delta}{A}}^{\pi+\arcsin\frac{\delta}{A}}\frac{kA}{\omega}(1-\cos\phi)\cos\phi d\phi+\int_{2\pi-\arcsin\frac{\delta}{A}}^{2\pi}\frac{kA}{\omega}(1-\cos\phi)\cos\phi d\phi\right]$$

$$=\frac{kA}{\pi\omega}\left[-\frac{2\delta}{A}\sqrt{1-\left(\frac{\delta}{A}\right)^2}-2\arcsin\frac{\delta}{A}\right]$$

$$=-\frac{2kA}{\pi\omega}\left[\frac{\delta}{A}\sqrt{1-\left(\frac{\delta}{A}\right)^2}+\arcsin\frac{\delta}{A}\right]$$

$b_1(\omega)=\frac{1}{\pi}\int_0^{2\pi} y(\phi)\cos\phi d\phi$

$$=\frac{1}{\pi}\left[\int_0^{\arcsin\frac{\delta}{A}}\frac{kA}{\omega}(1-\cos\phi)\sin\phi d\phi+\int_{\pi-\arcsin\frac{\delta}{A}}^{\pi+\arcsin\frac{\delta}{A}}\frac{kA}{\omega}(1-\cos\phi)\sin\phi d\phi+\int_{2\pi-\arcsin\frac{\delta}{A}}^{2\pi}\frac{kA}{\omega}(1-\cos\phi)\sin\phi d\phi\right]$$

$$=\frac{kA}{\pi\omega}[-\cos(\arcsin\frac{\delta}{A})+1+\frac{1}{4}\cos(2\arcsin\frac{\delta}{A})-\frac{1}{4}+\frac{1}{4}\cos(2\arcsin\frac{\delta}{A})$$

$$-\frac{1}{4}\cos(2\arcsin\frac{\delta}{A})-1+\cos(\arcsin\frac{\delta}{A})+\frac{1}{4}-\frac{1}{4}\cos(2\arcsin\frac{\delta}{A})]$$

=0

So, the D(A, ω)=[$b_1(\omega)$+j $a_1(\omega)$]/A=$-j\frac{2k}{\pi\omega}\left[\frac{\delta}{A}\sqrt{1-\left(\frac{\delta}{A}\right)^2}+\arcsin\frac{\delta}{A}\right]$

$$=\frac{2k}{\pi\omega}\left[\frac{\delta}{A}\sqrt{1-\left(\frac{\delta}{A}\right)^2}+\arcsin\frac{\delta}{A}\right]\angle-90^\circ \qquad (4.2.8)$$

It is derived from equation (4.2.8) that the nonlinear integrator's magnitude characteristic is a function of A and δ, and it has the same phase lag as the linear integrator.

4.2.3 Modified Nonlinear Integrator

The response of the modified nonlinear integrator to a sinusoidal input is shown below

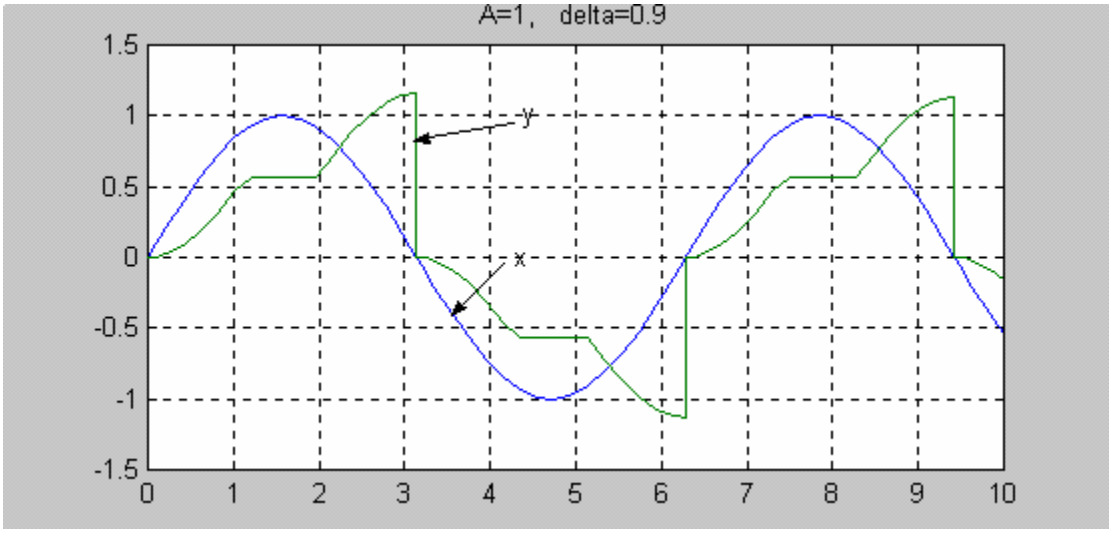

Figure 26. Sinusoidal response of Modified Nonlinear Integrator when A=1, δ=0.9

For the modified nonlinear integrator, if the input signal $x = A\sin\theta$, $\theta = \omega t$, the output of G-function is

$$z = \begin{cases} 0, & |\theta| > \arcsin\dfrac{\delta}{A} \\ kA\sin\theta, & |\theta| \le \arcsin\dfrac{\delta}{A} \end{cases} \qquad \delta > 0 \tag{4.2.9}$$

So, when $|\theta| \le \arcsin\dfrac{\delta}{A}$, the output of the integrator will be

$$y = \int_0^t kA\sin(\omega t)dt = \frac{kA}{\omega}\left(1-\cos(\omega t)\right) \tag{4.2.10}$$

The describing function is $D(A, \omega)=[b_1(\omega)+j\, a_1(\omega)]/A$

where $a_1(\omega)=\frac{2}{\pi}\int_0^{\pi} y(\phi)\cos\phi d\phi$

$$=\frac{2}{\pi}\left[\int_0^{\arcsin\frac{\delta}{A}}\frac{kA}{\omega}(1-\cos\phi)\cos\phi d\phi+\int_{\pi-\arcsin\frac{\delta}{A}}^{\pi}\frac{kA}{\omega}(1-\cos\phi)\cos\phi d\phi\right]$$

$$=\frac{2kA}{\pi\omega}\left[-\frac{1}{2}\sin(2\arcsin\frac{\delta}{A})-\arcsin\frac{\delta}{A}\right]$$

$$=-\frac{2kA}{\pi\omega}\left[\frac{\delta}{A}\sqrt{1-\left(\frac{\delta}{A}\right)^2}+\arcsin\frac{\delta}{A}\right]$$

$b_1(\omega)=\frac{2}{\pi}\int_0^{\pi} y(\phi)\sin\phi d\phi$

$$=\frac{2}{\pi}\left[\int_0^{\arcsin\frac{\delta}{A}}\frac{kA}{\omega}(1-\cos\phi)\sin\phi d\phi+\int_{\pi-\arcsin\frac{\delta}{A}}^{\pi}\frac{kA}{\omega}(1-\cos\phi)\sin\phi d\phi\right]$$

$$=\frac{4kA}{\pi\omega}[1-\sqrt{1-(\frac{\delta}{A})^2}]$$

So, $D(A, \omega)=[b_1(\omega)+ja_1(\omega)]/A$

$$=\frac{4k}{\pi\omega}[1-\sqrt{1-(\frac{\delta}{A})^2}]-j\frac{2k}{\pi\omega}\left[\frac{\delta}{A}\sqrt{1-\left(\frac{\delta}{A}\right)^2}+\arcsin\frac{\delta}{A}\right]$$

$$=\frac{2k}{\pi\omega}\sqrt{\left[2-2\sqrt{1-\left(\frac{\delta}{A}\right)^2}\right]^2+\left[\frac{\delta}{A}\sqrt{1-\left(\frac{\delta}{A}\right)^2}+\arcsin\frac{\delta}{A}\right]^2}$$

$$\angle arctg\frac{-\left(\arcsin\frac{\delta}{A}+\frac{\delta}{A}\sqrt{1-\left(\frac{\delta}{A}\right)^2}\right)}{2\left(1-\sqrt{1-\left(\frac{\delta}{A}\right)^2}\right)} \qquad (4.2.11)$$

It is derived from equation (4.2.11) that the modified nonlinear integrator's magnitude and phase characteristics are both functions of A and δ.

4.3 Integrators' Comparison According to Their Describing Functions

The amplitude and phase performances of various integrators, according to their describing functions, are shown in Figure 27 and Figure 28.

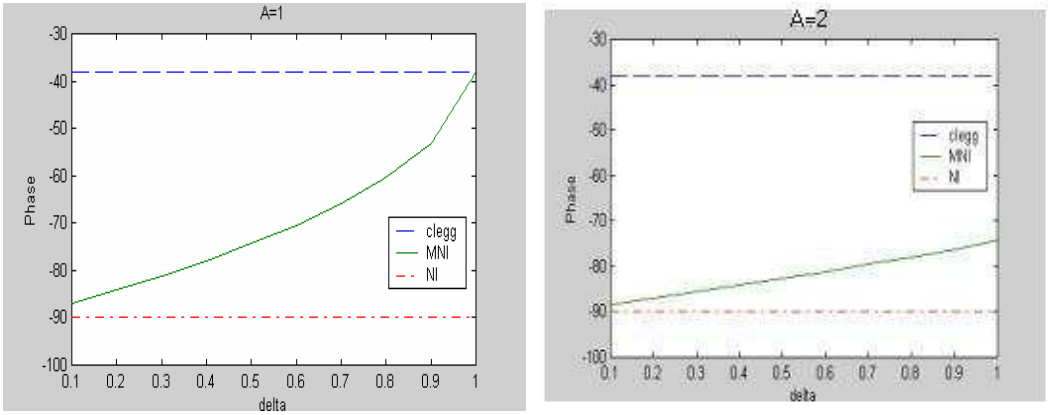

Figure 27. Integrators' phases for different δ when the amplitude of input signal A=1, 2

The above figures show that the phase lags of CI and NI are constant across all the δ values, while the phase lag of MNI increases with δ monotonically, with increasing rate depending on the amplitude of the input signal A.

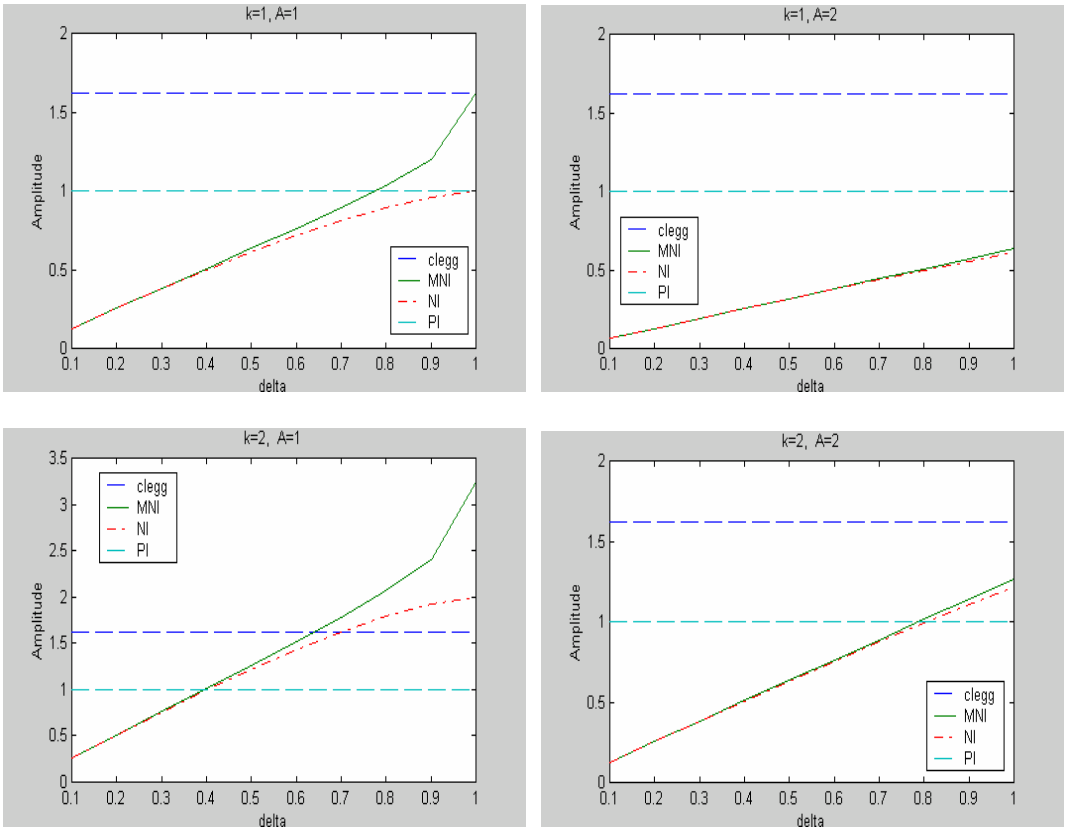

Figure 28 Integrators' amplitudes for different δ when the amplitude of input signal A=1, 2 and the slope of G-function k=1, 2

The above graphs demonstrate that the amplitudes of CI are all constant; while the amplitudes of NI and MNI increase with δ monotonically with a different rate, which is faster for larger k and slower for larger A.

From the above analysis it follows that the modified nonlinear integrator is better than the nonlinear integrator in both phase and amplitude response, but their phase advantages never exceed the phase of the Clegg Integrator.

4.4 Comparison in a Practical Application

For the model of the PWM DC-DC power converter in [16], we will separately apply linear proportional - linear integral controller (PI), linear proportional - nonlinear integral controller (PNI), linear proportional - Clegg integral controller (PCI) and linear proportional – modified nonlinear integral controller (PMI) to control it. The Simulink block diagram is shown in Figure 29. The plant transfer function [19] is

$$\frac{0.1569}{2.21\times10^{-7}s^2+7.52\times10^{-4}s+1} \tag{4.4.1}$$

There are two disturbance transfer functions. One is line voltage change transfer function:

$$\frac{4.84\times10^{-3}s+0.242}{3.52\times10^{-4}s^2+0.038s+1} \tag{4.4.2}$$

The other one is load current change transfer function:

$$\frac{0.075}{6.9\times10^{-7}s^2+1.2\times10^{-3}s+1} \tag{4.4.3}$$

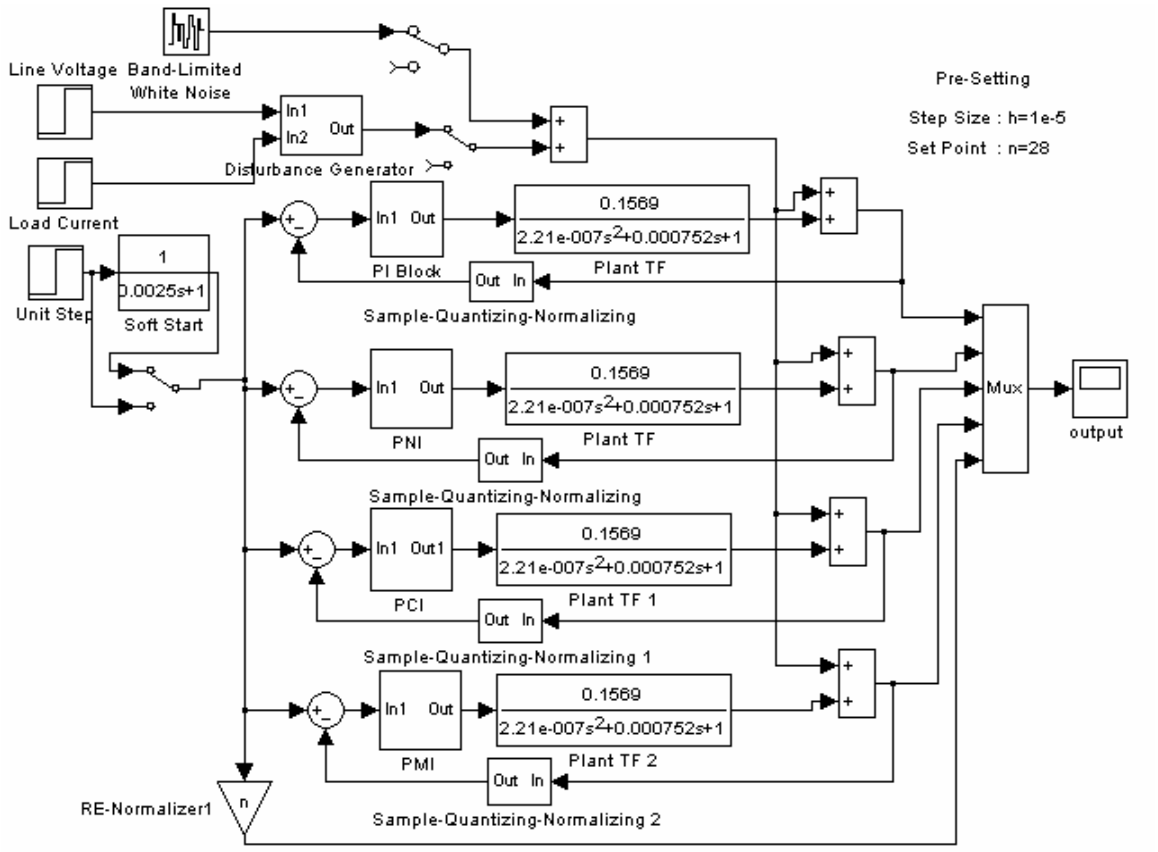

Figure 29. PI/PNI/PCI/PMI Simulation Blocks

The PI controller was developed previously [19]. The other three kinds of controllers are tuned here. Control gains are shown below:

PI: $k_p = 0.5$ $k_i = 800$

PNI: $k_p = 0.5$ $\begin{bmatrix} k_i = 1700 & \delta_i = 0.2 \\ k_{i1} = 1 & k_{i2} = -50 \end{bmatrix}$

PCI: $k_p = 0.5$ $k_i = 1400$

PMI: $k_p = 0.5$ $\begin{bmatrix} k_i = 1700 & \delta_i = 0.2 \\ k_{i1} = 1 & k_{i2} = -50 \end{bmatrix}$

4.4.1 Steady State Performance

When a soft start profile was used, there were no disturbance and no noise. The output voltage diagram is shown below for different controllers.

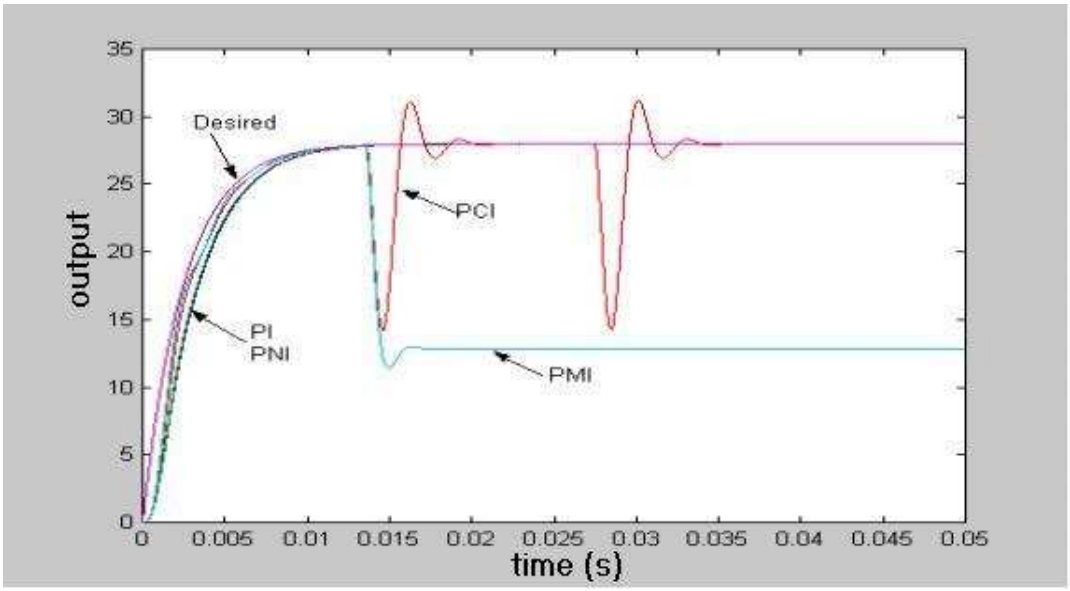

Figure 30. The nominal output responses for different controllers

From the above figure, it was observed that PMI and PCI controllers performed very badly, that is because their integrators need to be reset to zero when their input signals cross the zero. It is similar to a big disturbance applied to the system. The response of PMI is worse than that of PCI, because when it was reset to zero, the system generated a big error, and when this error was applied to the G-function, a small gain was output. It can not give the system enough control power, so there is a big steady-state error when using PMI as the controller. For PNI and PI controller, it is hard to tell which one is better from the above figure. The Correlation Coefficients were calculated in the following table to quantitatively evaluate the responses.

Table 7. The nominal output responses comparison for PI and PNI controllers

	PI	PNI
Correlation Coefficient	0.9932	0.9971

This table shows the PNI has the better performance. For the following sections, just PI and PNI are compared.

4.4.2 Line Disturbance Performance

When the line voltage is increased 30 volts from its nominal value of 120 volts and load current is kept as nominal 4 amps, the output results of PI, PNI controllers are shown below. The line disturbance is applied at 0.03s.

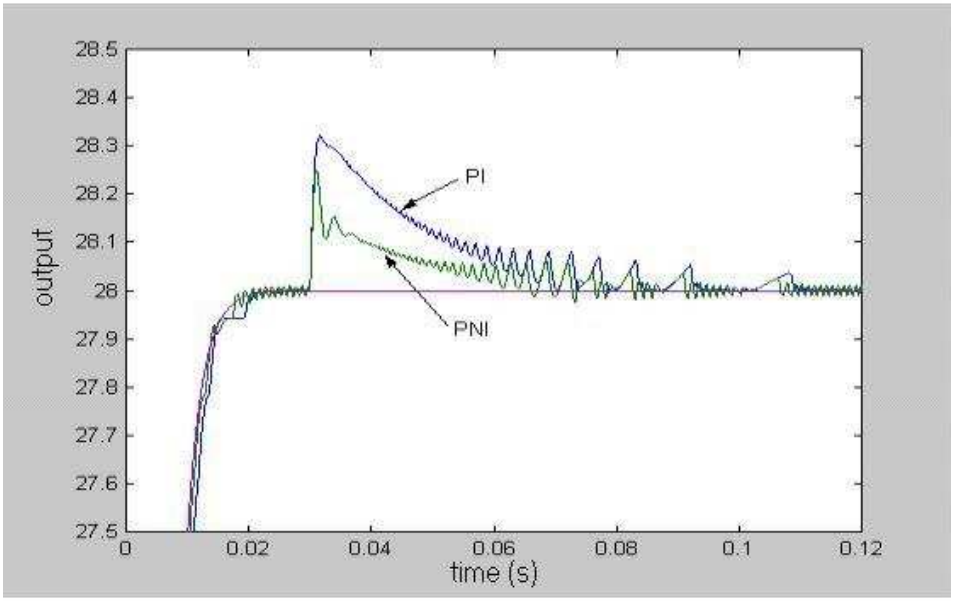

Figure 31. The output responses with line disturbance for PI and PNI controllers

From the above figure, it was observed that the PNI controller has better anti-line-disturbance performance than PI controller.

4.4.3 Load Disturbance Performance

When the load is increased from 4 amps to 36 amps and line voltage is kept at its nominal value of 120 volts, the output results of PI, PNI controllers are shown below. The load disturbance is applied at 0.03s.

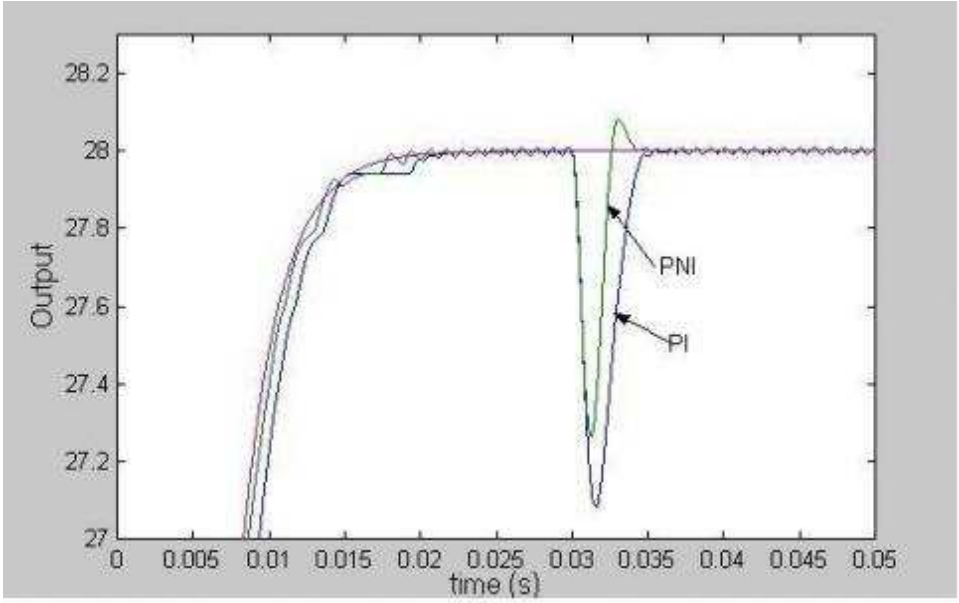

Figure 32. The output responses with load disturbance for different controllers

From the above figure, the PNI controller has better performance than PI.

4.4.4 Dual Disturbance Performance

This simulation is under dual disturbance conditions. The load current was increased 32 amps from its nominal value of 4 amps, while the line voltage was decreased 20 volts from its nominal supply voltage of 120 volts. This corresponds to a worst-case disturbance condition. Both line and load disturbances were applied at 0.03s.

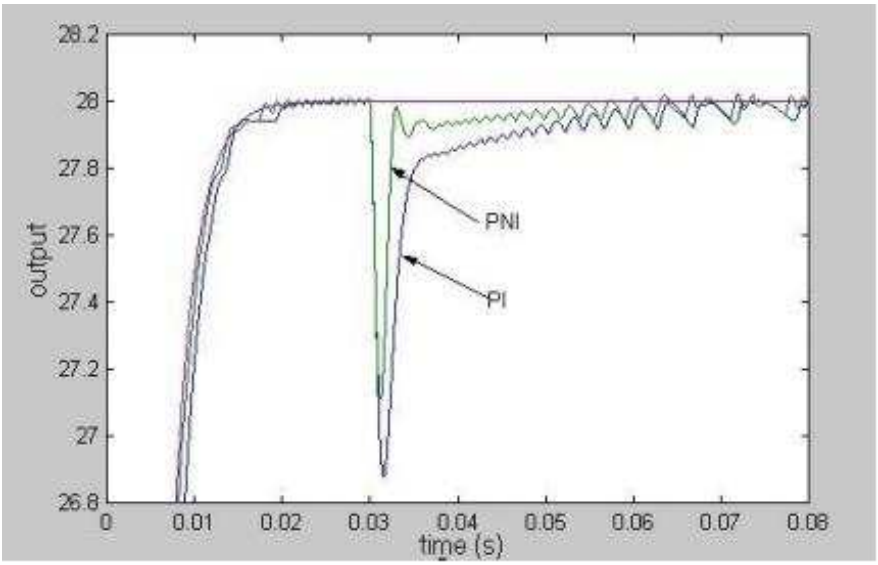

Figure 33. The output responses with dual disturbance for different controllers

From the above figure, the PNI controller has better performance than PI.

4.4.5 Noise Response

This simulation is under noise disturbance conditions. The load current was set to a nominal value of 4 amps, while the line voltage was set to a nominal supply voltage of 120 volts. The noise level was set to be $\pm 40\%$.

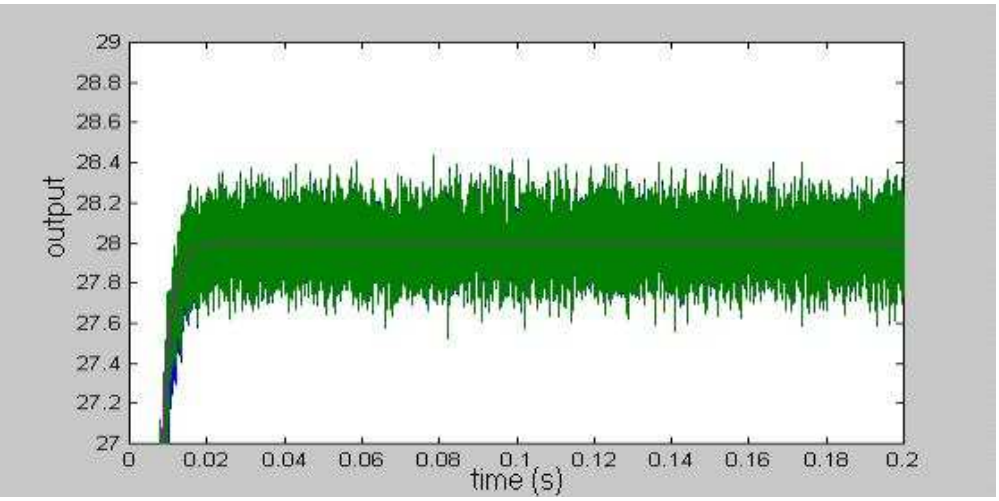

Figure 34. The output responses with noise disturbance for different controllers

Table 8. The output response comparison with noise disturbance for different controllers

	PI	PNI
Correlation Coefficient	0.9926	0.9962

It is hard to distinguish which one is better from Figure 33. But from the above table, the PNI controller has better performance than PI.

4.5 Summary

Although the Clegg Integrator has smaller phase lag than any other Integrator according to their Describing Function, its reset mechanism isn't suitable for some systems such as PWM DC-DC power converter. From the application before, it is clear that the Nonlinear Integrator has better performance than others for this case.

CHAPTER V

COMPARATIVE STUDY OF DIFFERENTIATORS IN A MOTION CONTROL SYSTEM

Motion control applications can be found in almost every sector of industry, from factory automation and robotics to high-tech computer hard-disk drives. They are used to regulate mechanical motions in terms of position, velocity, acceleration and/or to coordinate the motions of multiple axes or machine parts. A good differentiator is very useful for converting between position and velocity or between velocity and acceleration.

In this chapter, a powerful motion control law will be described by general mathematical derivation and example, then we will compare a classical linear second-order approximation differentiator and a nonlinear Tracking Differentiator in this example system.

5.1 Design Process for Motion Control System

A convenient model of the motion system can be derived via three steps:

(1) Using basic physical laws or first principles—Newton's Laws, Kirchhoff's Laws, conservation of mass, conservation of energy, etc—

to develop the form of a mathematical model that govern the behavior of devices and interconnection.

(2) Performing tests on the mechanism to determine values for the parameters in the model, and then

(3) Making final adjustments to the model's parameters so that its response (observed using simulation) matches as closely as possible the response of the actual mechanism.

In a typical application using a motor as the power source, the equation of motion can be described as by Newton's Law:

$$\ddot{y} = f(t, y, \dot{y}, w) + bu \tag{5.1.1}$$

where y is position, u is the motor current, b is the torque constant, and w represents the external disturbance such as vibrations and torque disturbances. The friction, the effect of inertia and various other nonlinearities in a motion system are all represented by the function $f(\cdot)$. Note that $f(\cdot)$ is generally a time-varying function. In most motion control literature, the linear, time-invariant, approximation is used:

$$\ddot{y} = \frac{c}{J}\dot{y} + \frac{b}{J}u \tag{5.1.2}$$

where J is the total inertia of the motor and load, and c is the viscous friction coefficient. This linear approximation allows the use of the transfer function $\mathrm{G(s)} = \dfrac{b}{s(Js+c)}$

Similar to other industrial control applications, proportional-integral-derivative (PID) control is the method of choice in most motion applications. A typical motion control scheme is shown in Figure 35, assuming both the position and velocity feedback

are available. The speed loop is usually controlled with a PI and the position loop with a simple proportional gain. The Simulink block diagram is shown below [21]:

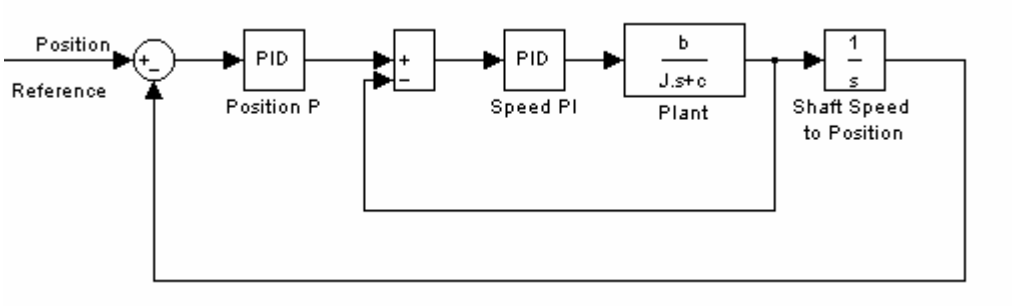

Figure 35. The block diagram of a motion control system

An intuitive design procedure is shown below.

5.1.1 Inner Loop Design

The speed loop controller is chosen as a PI controller of the form

$$C(s) = \frac{K_{SP}s + K_{SI}}{s} \tag{5.1.3}$$

The closed loop transfer function for the inner loop is

$$\mathrm{F(s)} = \frac{C(s)G(s)}{1 + C(s)G(s)} = \frac{\dfrac{K_{SP}s + K_{SI}}{s} \cdot \dfrac{b}{Js + c}}{1 + \dfrac{K_{SP}s + K_{SI}}{s} \cdot \dfrac{b}{Js + c}}$$

$$= \frac{s + \dfrac{K_{SI}}{K_{SP}}}{\dfrac{J}{K_{SP}b}s^2 + (\dfrac{c}{K_{SP}b} + 1)s + \dfrac{K_{SI}}{K_{SP}}} \tag{5.1.4}$$

which can be simplified by selecting the controller parameters carefully. That is,

$$\mathrm{F(s)} = \frac{s + \dfrac{K_{SI}}{K_{SP}}}{(\dfrac{J}{K_{SP}b}s + 1)(s + \dfrac{K_{SI}}{K_{SP}})} = \frac{1}{\dfrac{J}{K_{SP}b}s + 1} = \frac{1}{\dfrac{1}{\omega_c}s + 1} \tag{5.1.5}$$

if $\frac{c}{K_{SP}b} = \frac{J}{K_{SP}b} \cdot \frac{K_{SI}}{K_{SP}}$, i.e. $c = J\frac{K_{SI}}{K_{SP}} \Rightarrow K_{SI} = \frac{c}{J}K_{SP}$ (5.1.6)

where $\omega_c = \frac{K_{SP}b}{J}$, the bandwidth of the speed loop. Thus K_{SP} and K_{SI} are determined as

$$K_{SP} = \frac{J}{b}\omega_c, \quad K_{SI} = \frac{c}{b}\omega_c \tag{5.1.7}$$

5.1.2 The Effect of Inertia Change in the Inner Loop

When total inertia *J* is changed by a factor of *k*, it can be shown that the inner loop transfer function F(s) is still approximately first order system as seen in (5.1.5), i.e.

$$\frac{s + \frac{K_{SI}}{K_{SP}}}{\frac{J}{K_{SP}b}s^2 + (\frac{c}{K_{SP}b} + 1)s + \frac{K_{SI}}{K_{SP}}} \approx \frac{1}{\frac{s}{\omega_c} + 1} \tag{5.1.8}$$

This is because, in the left side of equation, there is always a pole that can almost cancel its zero. In this case, $\omega_c = \frac{K_{SP}b}{\bar{J}}$, where $\bar{J}$ is the average inertia defined as

$$\bar{J} = \frac{J_{\min} + J_{\max}}{2} \tag{5.1.9}$$

Here $J_{\min}$ is the minimum total inertia, $J_{\max}$ is the maximum total inertia and

$$J_{\max} = kJ_{\min}. \tag{5.1.10}$$

Obviously,

$$J_{\min} = \frac{2}{k+1}\bar{J} \text{ and } J_{\max} = \frac{2k}{k+1}\bar{J} \tag{5.1.11}$$

The poles of the left side of equation (5.1.8) are:

$$P_{1,2} = \frac{-\left(\frac{c}{K_{SP}b}+1\right) \pm \sqrt{\left(\frac{c}{K_{SP}b}+1\right)^2 - 4\cdot\frac{J}{K_{SP}b}\cdot\frac{K_{SI}}{K_{SP}}}}{2\cdot\frac{J}{K_{SP}b}}$$

$$= \frac{-\left(c+K_{SP}b\right) \pm \sqrt{\left(c+K_{SP}b\right)^2 - 4JK_{SI}b}}{2J} \tag{5.1.12}$$

With $K_{SP} = \frac{\overline{J}}{b}\omega_c$, $K_{SI} = \frac{c}{b}\omega_c$, (5.1.12) can be rewritten as

$$P_{1,2} = \frac{-\left(c+\overline{J}\omega_c\right) \pm \sqrt{\left(c+\overline{J}\omega_c\right)^2 - 4Jc\omega_c}}{2J} \tag{5.1.13}$$

The zero of the left side of equation (5.1.8) is

$$Z = -\frac{K_{SI}}{K_{SP}} = -\frac{\frac{c}{b}\omega_c}{\frac{\overline{J}}{b}\omega_c} = -\frac{c}{\overline{J}} \tag{5.1.14}$$

When $J = \overline{J}$, $\overline{P_1} = \frac{-\left(c+\overline{J}\omega_c\right) + \sqrt{\left(c+\overline{J}\omega_c\right)^2 - 4\overline{J}c\omega_c}}{2\overline{J}} = -\frac{c}{\overline{J}}$

$$\overline{P_2} = \frac{-\left(c+\overline{J}\omega_c\right) - \sqrt{\left(c+\overline{J}\omega_c\right)^2 - 4\overline{J}c\omega_c}}{2\overline{J}} = -\omega_c \tag{5.1.15}$$

Obviously $\overline{P_1}$ and Z are canceled each other and (5.1.8) holds.

When $J = J_{\min} = \frac{2}{k+1}\overline{J}$,

$$\frac{P_{1\min}}{\overline{P_1}} = \frac{\frac{-\left(c+\overline{J}\omega_c\right) + \sqrt{\left(c+\overline{J}\omega_c\right)^2 - \frac{8}{k+1}\overline{J}c\omega_c}}{\frac{4}{k+1}\overline{J}}}{-\frac{c}{\overline{J}}}$$

$$= \frac{\frac{k+1}{4}\left(c+\bar{J}\omega_c\right) - \frac{k+1}{4}\sqrt{c^2+\left(2-\frac{8}{k+1}\right)\bar{J}c\omega_c+\left(\bar{J}\omega_c\right)^2}}{c} \tag{5.1.16}$$

Because $\left|c^2+\left(2-\frac{8}{k+1}\right)\bar{J}c\omega_c\right| \gg \left(\bar{J}\omega_c\right)^2$, then $\frac{P_{1\min}}{\bar{P}_1} \approx \frac{\frac{k+1}{4}\left(c+\bar{J}\omega_c\right)-\frac{k+1}{4}\bar{J}\omega_c}{c} = \frac{k+1}{4}$,

i.e., $P_{1\min} = \frac{k+1}{4}\bar{P}_1$. (5.1.17)

When $J = J_{\max} = \frac{2k}{k+1}\bar{J}$,

$$\frac{P_{1\max}}{\bar{P}_1} = \frac{\frac{-\left(c+\bar{J}\omega_c\right)+\sqrt{\left(c+\bar{J}\omega_c\right)^2-\frac{8k}{k+1}\bar{J}c\omega_c}}{\frac{4k}{k+1}\bar{J}}}{-\frac{c}{\bar{J}}}$$

$$= \frac{\left(c+\bar{J}\omega_c\right)-\sqrt{c^2+\frac{2-6k}{k+1}\bar{J}c\omega_c+\left(\bar{J}\omega_c\right)^2}}{\frac{4k}{k+1}c} \tag{5.1.18}$$

Because $\left|c^2+\frac{2-6k}{k+1}\bar{J}c\omega_c\right| \gg \left(\bar{J}\omega_c\right)^2$, then $\frac{P_{1\max}}{\bar{P}_1} \approx \frac{\left(c+\bar{J}\omega_c\right)-\bar{J}\omega_c}{\frac{4k}{k+1}c} = \frac{k+1}{4k}$,

i.e., $P_{1\max} = \frac{k+1}{4k}\bar{P}_1$. (5.1.19)

When $\bar{P}_1$ is very small, $P_{1\max}$ and $P_{1\min}$ both are very small. Comparing to their second poles, $P_{1\max}$ and $P_{1\min}$ both are very close to $\bar{P}_1$ and the zero can cancel them. In summary, the pole-zero in cancellation (5.1.8) is still a valid approximation when inertia is changed by a factor of *k*.

5.1.3 The Bandwidth of the System with Unity Feedback Loop

With the inner speed loop design in equation (5.13) to (5.18), the motion control system in Figure 35 can now be redrawn as

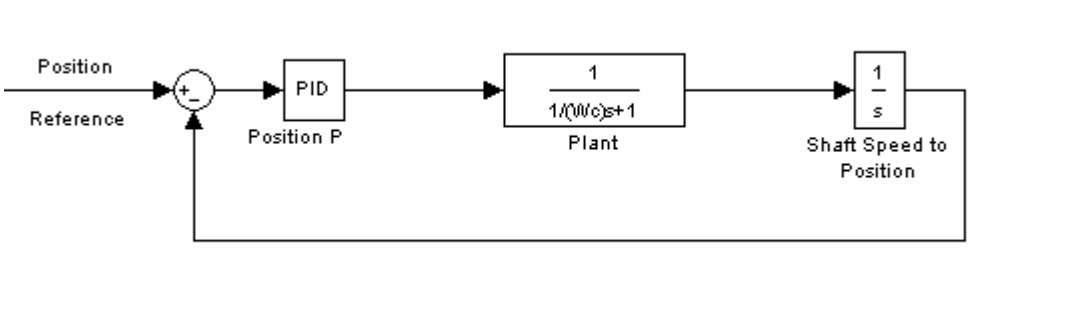

Figure 36. Simplified block diagram of the motion control system

When a proportional controller is used as the position loop controller, the closed loop transfer function is

$$\text{TF} = \frac{K_p \cdot \dfrac{1}{s(s/\omega_c + 1)}}{1 + \dfrac{K_p}{s(s/\omega_c + 1)}} = \frac{1}{\dfrac{s^2}{\omega_c K_p} + \dfrac{1}{K_p} S + 1} \tag{5.1.20}$$

The standard second order system is

$$\frac{\omega_n^2}{s^2 + 2\xi\omega_n s + \omega_n^2} = \frac{1}{\dfrac{s^2}{\omega_n^2} + \dfrac{2\xi}{\omega_n} s + 1} \tag{5.1.21}$$

By comparing equations (5.1.20) and (5.1.21), equation (5.1.22) is derived:

$$\begin{cases} \omega_c K_p = \omega_n^2 \\ \dfrac{1}{K_p} = \dfrac{2\xi}{\omega_n} \end{cases} \Rightarrow \begin{cases} \omega_n = \sqrt{\omega_c K_p} \\ \xi = \dfrac{\omega_n}{2K_p} = \sqrt{\dfrac{\omega_c}{4K_p}} \end{cases} \tag{5.1.22}$$

The bandwidth ω_b of standard second order system is defined as

$$\left| \frac{\omega_n^2}{(j\omega)^2 + 2\xi\omega_n(j\omega) + \omega_n^2} \right|_{\omega=\omega_b} = 0.707$$

$$\Rightarrow \omega_b = \omega_n \sqrt{\left(1 - 2\xi^2\right) + \sqrt{2 - 4\xi^2 + 4\xi^4}} \tag{5.1.23}$$

The relationship of ξ and ω_b / ω_n is shown in Figure 37. It is decreasing with ξ monotonically.

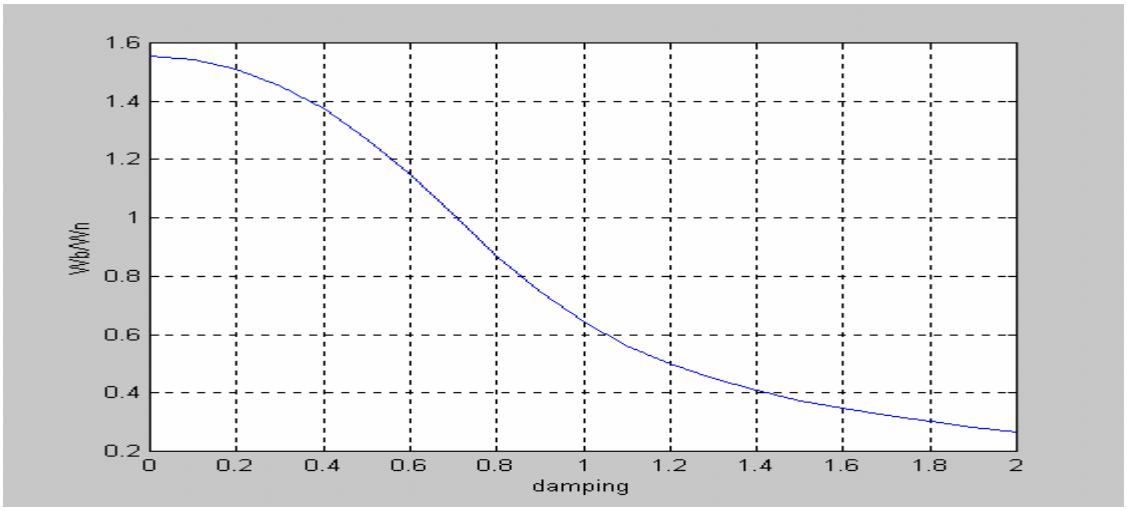

Figure 37. The relationship of ξ and ω_b / ω_n

Assume $0 < \xi \leq 1$,

$$\sqrt{(1-2) + \sqrt{2 - 4 + 4}} < \frac{\omega_b}{\omega_n} \leq \sqrt{1 + \sqrt{2}}$$

$$\Rightarrow \sqrt{0.414}\omega_n < \omega_b \leq \sqrt{2.414}\omega_n$$

$$\Rightarrow \sqrt{0.414\omega_c K_p} < \omega_b \leq \sqrt{2.414\omega_c K_p} \tag{5.1.24}$$

From equation (5.1.22), it follows that

$$0 < \sqrt{\frac{\omega_c}{4K_p}} \le 1 \Rightarrow K_p \ge \frac{1}{4}\omega_c$$

For the sake of simplicity, Let $K_p = \frac{1}{4}\omega_c$ (5.1.25)

Equation (5.1.24) becomes

$$\sqrt{0.1035}\omega_c < \omega_b \le \sqrt{0.6035}\omega_c$$

$$\Rightarrow 0.32\omega_c < \omega_b \le 0.78\omega_c \quad (5.1.26)$$

This indicates the bandwidth of position loop varies from $0.32\omega_c$ to $0.78\omega_c$ when assuming $0 < \xi \le 1$, which is a common practice.

5.1.4 The Effect of Using Feedback Forcing

If feedback forcing is added and the feedback lead/lag frequencies are determined in the following way: the numerator, i.e. lead part, is set to approximately cancel the instantaneous closed speed loop lag, while the denominator, i.e. lag part frequency, is set at about ten times the lead part frequency. The consequent transfer function of compensative component is [21]:

$$\frac{1/\omega_c s + 1}{1/(10\omega_c)s + 1} \quad (5.1.27)$$

Thus, the block diagram of the motion control system becomes

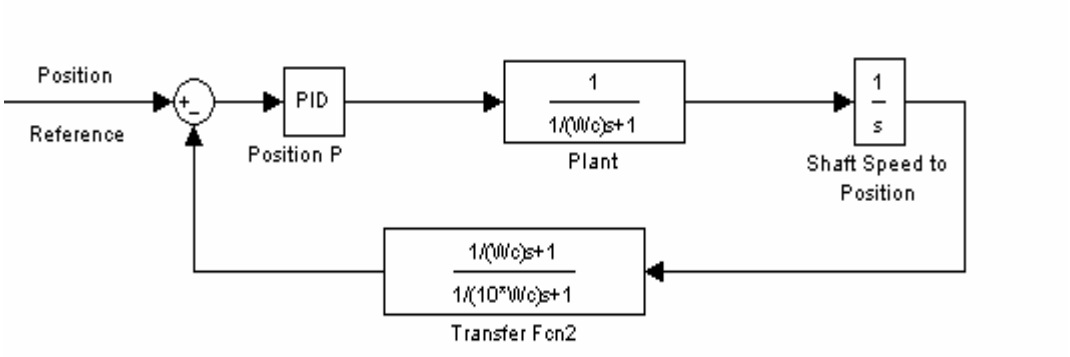

Figure 38. The block diagram of the system with feedback forcing

The transfer function of this closed position loop system is

$$G_{cl}(s) = \frac{K_p \cdot \dfrac{1}{s(s/\omega_c + 1)}}{1 + \dfrac{K_p}{s(s/10\omega_c + 1)}}$$

$$= \frac{K_p}{s(\dfrac{1}{\omega_c}s + 1) + \dfrac{K_p(\dfrac{1}{\omega_c}s + 1)}{\dfrac{1}{10\omega_c}s + 1}} \qquad (5.1.28)$$

$\dfrac{1}{10\omega_c}$ is a very small number, which can be set to zero for simplification. Then

$$G_{cl}(s) = \frac{K_p}{\dfrac{1}{\omega_c}s^2 + (\dfrac{K_p}{\omega_c} + 1)s + K_p} = \frac{1}{\dfrac{1}{\omega_c K_p}s^2 + \left(\dfrac{1}{\omega_c} + \dfrac{1}{K_p}\right)s + 1}$$

$$= \frac{1}{\left(\dfrac{s}{\omega_c} + 1\right)\left(\dfrac{s}{K_p} + 1\right)} \qquad (5.1.29)$$

When K_p was set as $\frac{1}{4}\omega_c$, it is the more dominant pole of the transfer function. It is unaffected by the inertia change. Thus, the bandwidth of the system with feedback forcing is approximately $0.25\,\omega_c$.

In conclusion, the use of feedback forcing helps to reduce the effect of inertia change on the closed-loop system. The position controller, K_p, should be selected following equation (5.1.25).

5.2 Simulation Study of an Industrial Motion System

This system includes a PC based control platform and a DC brushless servo system made by ECP (model 220) [13]. The servo system includes two motors, one is an actuator, and the other is the disturbance source. The mathematical model of this motion system has been derived and verified in hardware test in [15]. The transfer function of this plant takes the form:

$$G(s)=\frac{16.5}{s(Js+1)} \tag{5.2.1}$$

The Simulink block diagram is shown below:

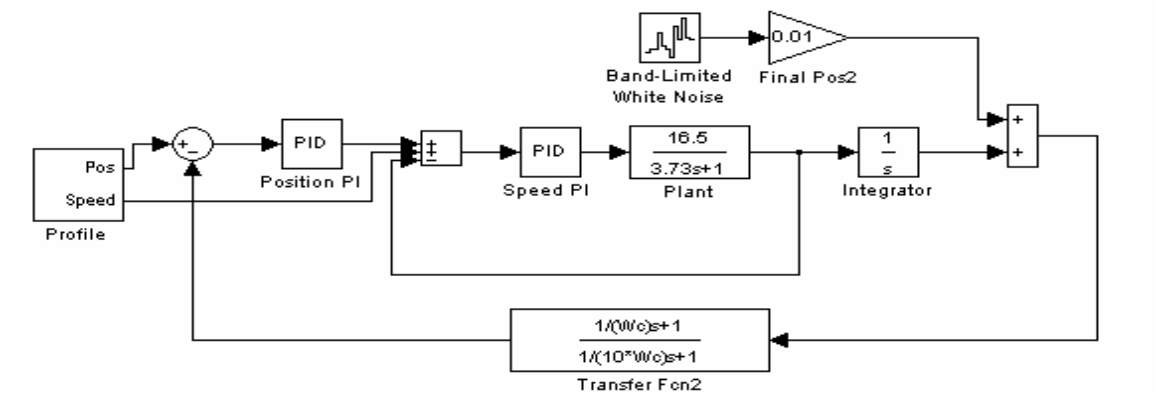

Figure 37. Simulation in a motion control system

First, Determining K_{SP}, K_{SI} and K_p. Because the inertia J of plant will change from $J_{\min}$=0.35 to $J_{\max}=7.1$, the average inertia $\bar{J}$=(0.35+7.1)/2=3.73 is used. With b=16.5, c=1, from equation (5.1.7) and (5.1.25), $K_{SP}=\frac{\bar{J}}{b}\omega_c=\frac{3.73}{16.5}\omega_c=0.23\omega_c$, $K_{SI}=\frac{c}{b}\omega_c=\frac{1}{16.5}\omega_c=0.06\omega_c$, $K_p=\frac{1}{4}\omega_c$. The parameter to be tuned is ω_c. After iterative tuning in the simulation, ω_c was set to 30.

Next, verify the inner-loop poles. The inner speed loop transfer function is:

$$\mathrm{F(s)}=\frac{C(s)G(s)}{1+C(s)G(s)}=\frac{s+\frac{K_{SI}}{K_{SP}}}{\frac{J}{K_{SP}b}s^2+(\frac{c}{K_{SP}b}+1)s+\frac{K_{SI}}{K_{SP}}} \tag{5.2.2}$$

The zero of this equation is

$$Z=-\frac{K_{SI}}{K_{SP}}=-\frac{c}{\bar{J}}=-\frac{1}{3.73}=-0.268 \tag{5.2.3}$$

The poles of this equation are:

$$P_{1,2}=\frac{-\left(c+\bar{J}\omega_c\right)\pm\sqrt{\left(c+\bar{J}\omega_c\right)^2-4Jc\omega_c}}{2J}$$

$$=\frac{-\left(1+3.73\times30\right)\pm\sqrt{\left(1+3.73\times30\right)^2-4\times30J}}{2J}$$

$$=\frac{-112.9\pm\sqrt{12746.41-120J}}{2J} \tag{5.2.4}$$

When $J=\bar{J}=3.73$,

$$\bar{P}_{1,2}=\frac{-112.9\pm\sqrt{12746.41-120\times3.73}}{2\times3.73}=\frac{-112.9\pm110.9}{7.46}$$

$$\Rightarrow \begin{cases} \overline{P}_1 = \dfrac{-1}{3.73} = -0.268 \\ \overline{P}_2 = \dfrac{-223.8}{7.46} = -30 \end{cases} \tag{5.2.5}$$

When $J = J_{\min} = 0.35$,

$$P_{1,2\min} = \frac{-112.9 \pm \sqrt{12746.41 - 120 \times 0.35}}{2 \times 0.35} = \frac{-112.9 \pm 112.7}{0.7}$$

$$\Rightarrow \begin{cases} P_{1\min} = \dfrac{-0.2}{0.7} = -0.286 \\ P_{2\min} = \dfrac{-225.6}{0.7} = -322.29 \end{cases} \tag{5.2.6}$$

When $J = J_{\max} = 7.1$,

$$P_{1,2\max} = \frac{-112.9 \pm \sqrt{12746.41 - 120 \times 7.1}}{2 \times 7.1} = \frac{-112.9 \pm 109.06}{14.2}$$

$$\Rightarrow \begin{cases} P_{1\max} = \dfrac{-3.84}{14.2} = -0.270 \\ P_{2\max} = \dfrac{-221.96}{14.2} = -15.63 \end{cases} \tag{5.2.7}$$

Thus, the pole P_1 is very close to the zero, it can always be canceled by the zero. Then the inner speed loop transfer function can be simplified as

$$\mathrm{F(s)} = \frac{1}{\dfrac{1}{\omega_c} s + 1} \tag{5.2.8}$$

Finally, evaluate the system with feedback forcing. The responses of this system are compared as inertia varied. Figure 40 – Figure 41 show the normal responses and measurement noise responses of this system when inertia $J_{\min}$ equals 0.35. Figure 42-

Figure 43 show the normal responses and measurement noise responses of this system when inertia $J_{\max}$ equals 7.1.

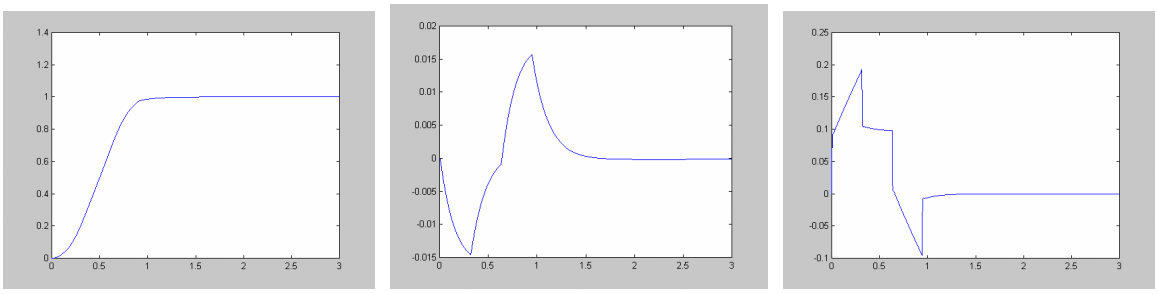

Position response Error response Control signal response

Figure 40. The normal responses when inertia $J_{\min}$ equals 0.35

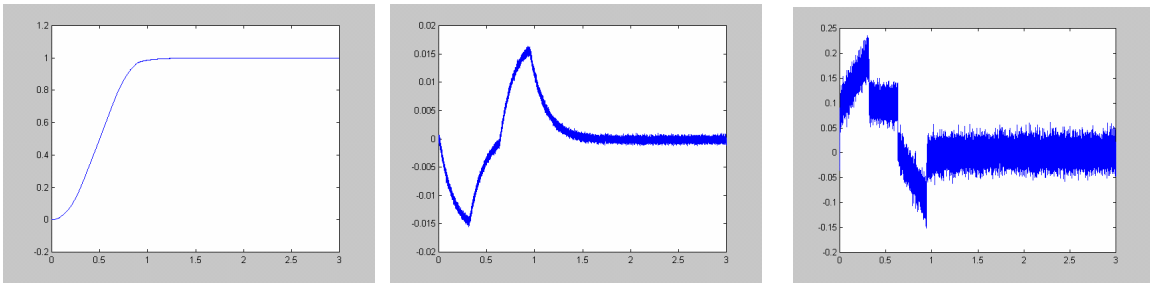

Position response Error response Control signal response

Figure 41. The measurement noise (0.01%) responses when inertia $J_{\min}$ equals 0.35

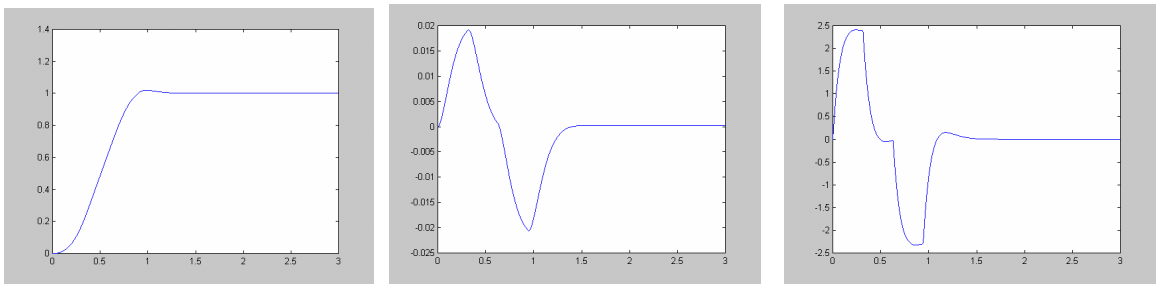

Position response Error response Control signal response

Figure 42. The normal responses when inertia $J_{\max}$ equals 7.1

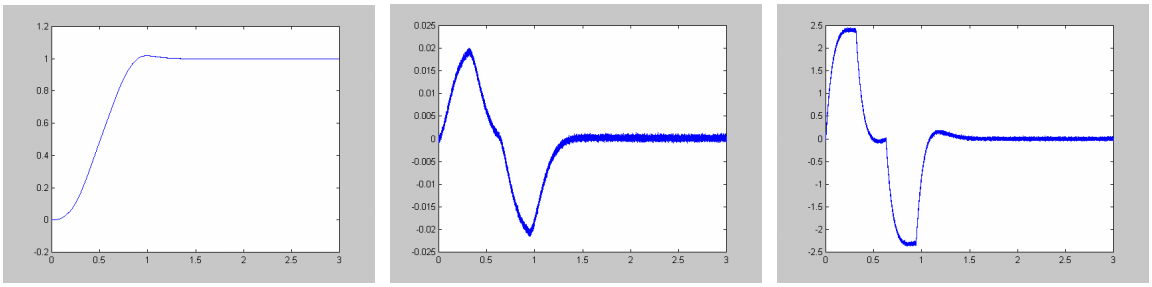

Position response Error response Control signal response

Figure 43. The measurement noise (0.01%) responses when inertia $J_{\max}$ equals 7.1

The above figures show that the proposed controller produces constant output response as the inertia changes by a factor of 20.

5.3 The Comparison of the Motion Control System with or without Position Loop Feedback Forcing

In this section, we compare the motion control system with or without position loop feedback forcing in frequency domain and time domain.

For the position loop without feedback forcing, the open loop transfer function of the system is:

$$L_1(s) = K_p \cdot \frac{1}{s} \frac{s + \frac{K_{SI}}{K_{SP}}}{\frac{J}{K_{SP}b} s^2 + \left(\frac{c}{K_{SP}b} + 1 \right) s + \frac{K_{SI}}{K_{SP}}}$$

$$= \frac{\frac{1}{4}\omega_c \left(s + \frac{c}{\bar{J}} \right)}{\frac{J}{\bar{J}\omega_c} s^3 + \left(\frac{c}{\bar{J}\omega_c} + 1 \right) s^2 + \frac{c}{\bar{J}} s} \qquad (5.3.1)$$

When $\omega_c = 30$, $\bar{J}$ =3.73, c=1

$$L_1(s) = \frac{7.5s + 2.01}{\frac{J}{111.9}s^3 + 1.009s^2 + 0.268s} \tag{5.3.2}$$

For the position loop with feedback forcing, the open loop transfer function of the system is:

$$L_2(s) = L_1(s) \cdot \frac{\frac{1}{\omega_c}s + 1}{\frac{1}{10\omega_c}s + 1} \tag{5.3.3}$$

When $\omega_c = 30$,

$$L_2(s) = \frac{7.5s + 2.01}{\frac{J}{111.9}s^3 + 1.009s^2 + 0.268s} \cdot \frac{0.03s + 1}{0.003s + 1} \tag{5.3.4}$$

Their Bode diagrams are shown below for different inertias. Their phase margins and bandwidths are list in Table 9. The bandwidth of the system with feedback forcing is wider than that of the system without feedback forcing and the phase margin of the system with feedback forcing is bigger than the system without feedback forcing.

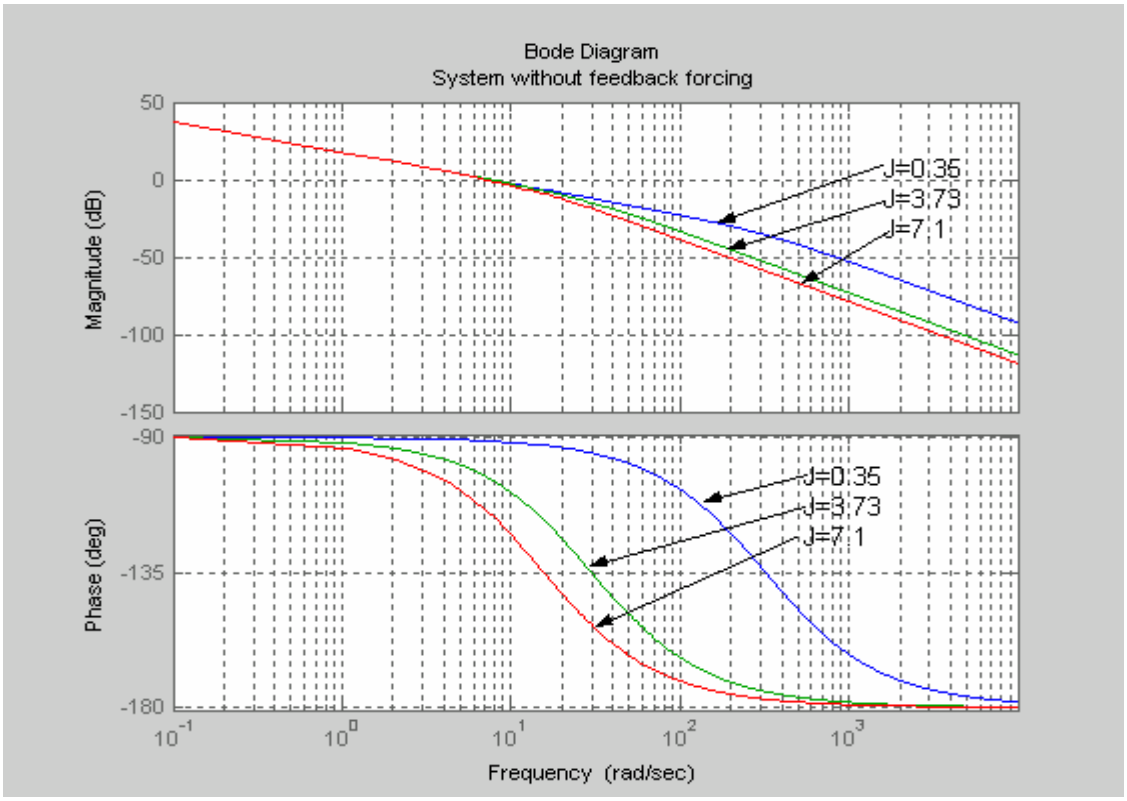

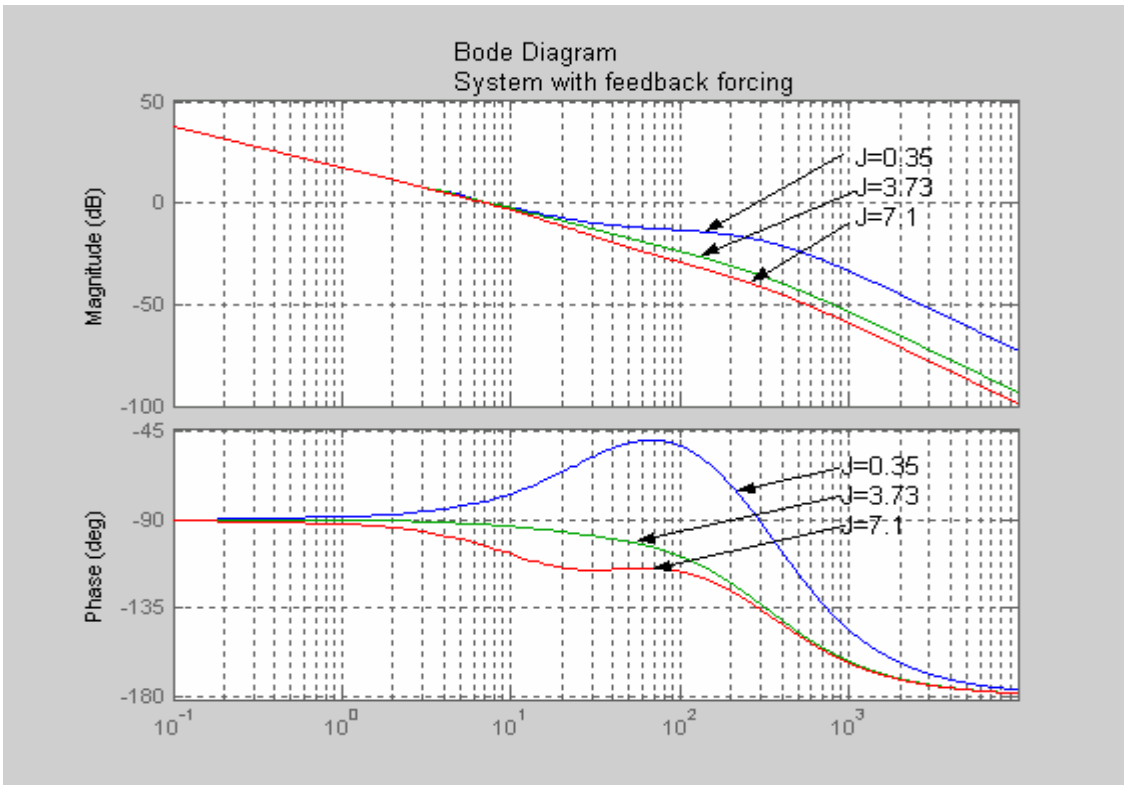

Figure 44. The frequency responses of the systems with and without feedback forcing

Table 9. The phase margins and bandwidths of the systems with and without feedback forcing

	J=0.35	J=3.73	J=7.1
System without Feedback forcing	Pm=88.661°	Pm=76.347°	Pm=66.155°
	BW=7.4373 rad/sec	BW=7.2876 rad/sec	BW=6.9151 rad/sec
System with Feedback forcing	Pm=100.21°	Pm=87.371°	Pm=76.482°
	BW=7.6275 rad/sec	BW=7.4561 rad/sec	BW=7.4561 rad/sec

The systems with and without feedback forcing were compared above in frequency domain. Then they will be compared in time-domain.

The simulation block diagram is shown below:

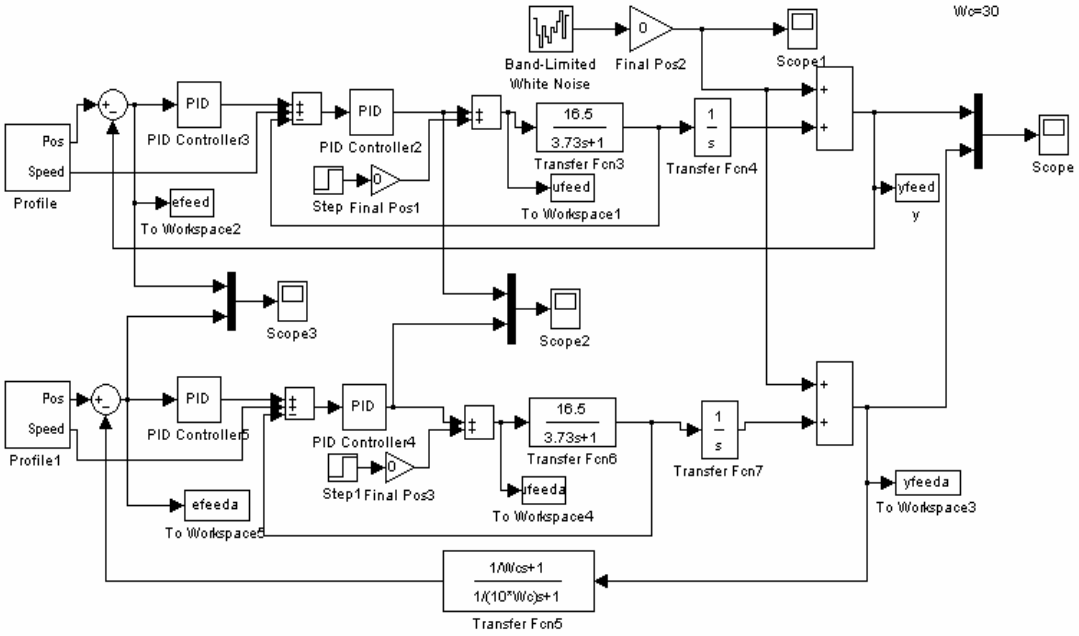

Figure 45. Comparing the systems with and without feedback forcing

In the following simulations, position, error and control signal responses of the above system are compared under these conditions:

1. With and without position loop feedback forcing

2. With inertia set to 0.35, 3.73 and 7.1, respectively

3. With and without disturbance.

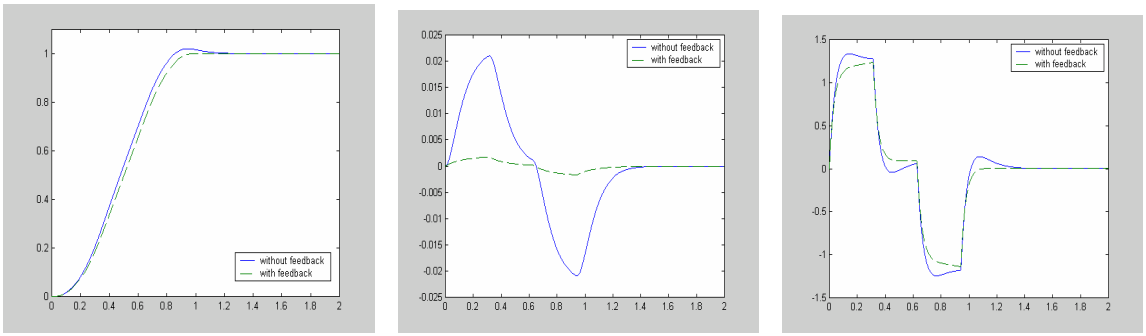

Position response Error response Control signal response

Figure 46. The responses of the system with and without position loop feedback forcing when inertia J =3.73 and no disturbance

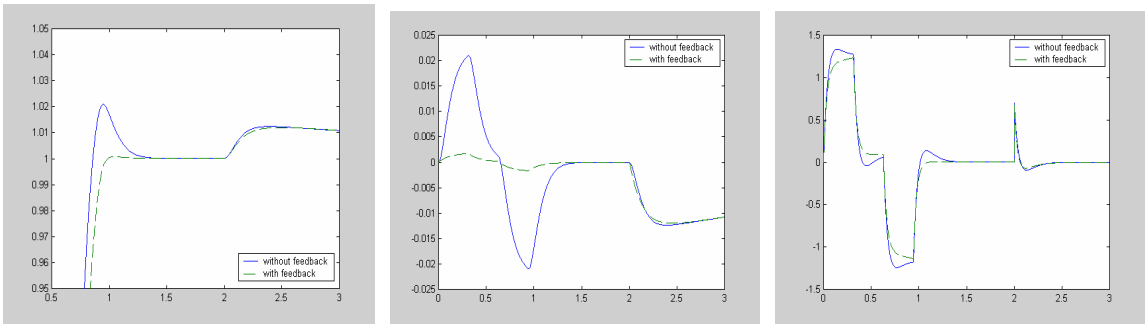

Position response Error response Control signal response

Figure 47. The responses of the system with and without position loop feedback forcing when inertia J =3.73 and with disturbance

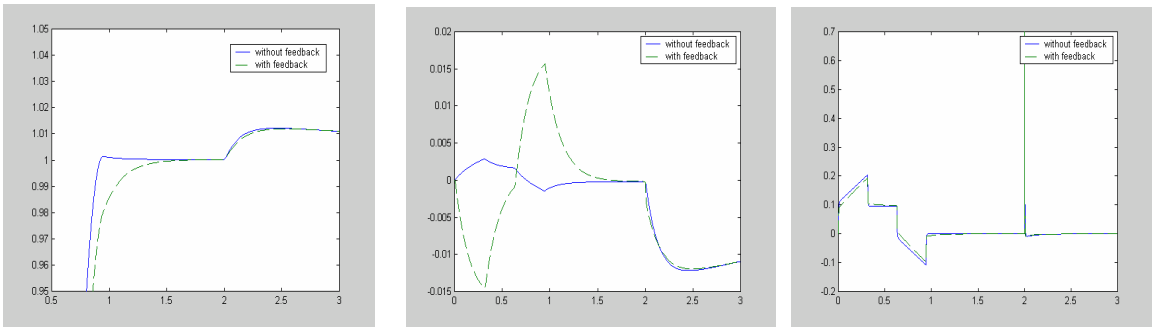

Position response Error response Control signal response

Figure 48. The responses of the system with and without position loop feedback forcing when inertia J =0.35 and with disturbance

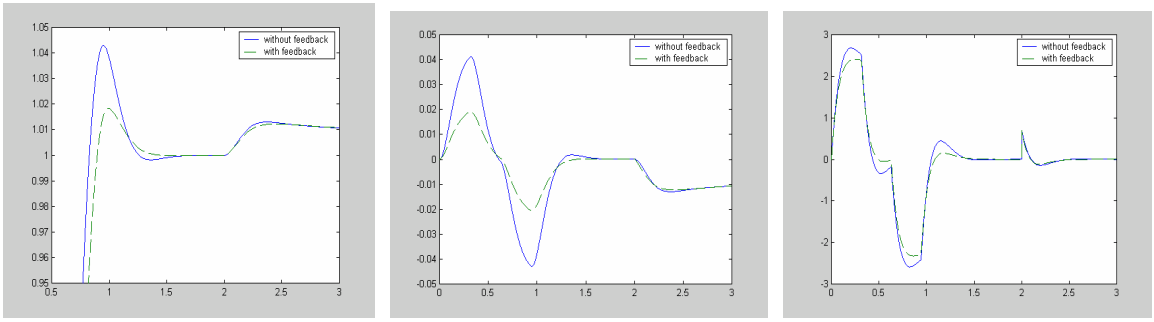

Position response Error response Control signal response

Figure 49. The responses of the system with and without position loop feedback forcing when inertia J =7.1 and with disturbance

From Figure 46 – Figure 49, it is clear when inertia changes from 0.35 to 7.1, the error of the system with feedback forcing is always below $\pm 2\%$, but the error of system without feedback forcing sometime reaches 4%. When inertia is bigger, the position response of system with feedback forcing has smaller overshoot than the system without feedback forcing.

Summary

The use of inner loop greatly improves the performance when inertia is changed and the use of the feedback forcing helps to reduce the error from 4% to 2% and improve the phase margin by about 10 degrees. At the same time, controller tuning is simplified to adjust only one parameter, ω_c .

5.4 Closing Velocity Loop Using Approximated Differentiator

In the previous section, the velocity loop of the motion control system is closed using ideal velocity feedback. In this section, the NTD and LA2 are used in this system to get the approximate velocity feedback. The position, position error and control signal of the system are compared. The simulation setup is shown below.

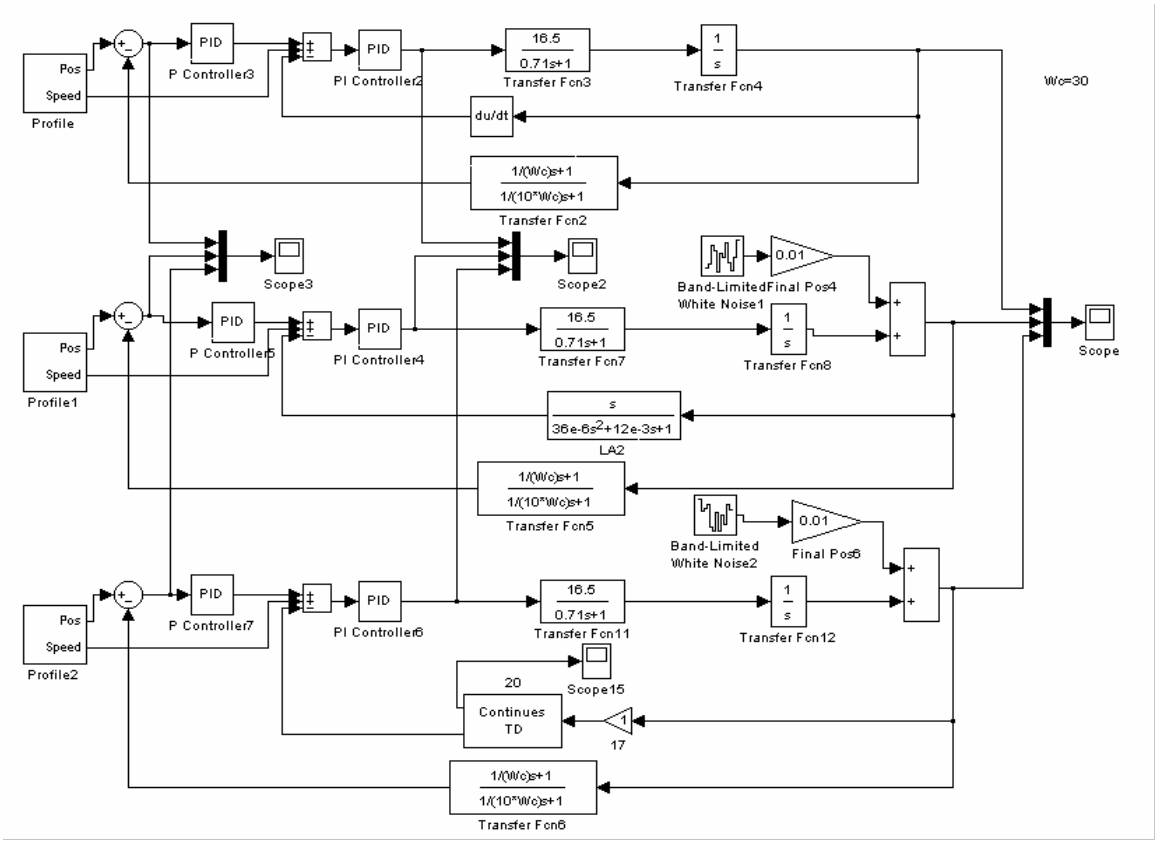

Figure 50. Comparing differentiators in a motion control system

The parameters of the system are:

Speed PI controller: $K_{SP} = 0.23\omega_c$, $K_{SI} = 0.06\omega_c$

Position controller: $K_p = \frac{1}{4}\omega_c$

LA2: $\tau = 0.006$

NTD: $R = 60$, $h = 0.001$

The parameters of the PI controller and the P controller are kept the same as the last section; while the parameters of the LA2 and NTD are tuned to make the outputs as close as possible to the output of the ideal differentiator, and make the system noise-resistant. The normal responses are shown in Figure 51 and the measurement noise responses are shown in Figure 52.

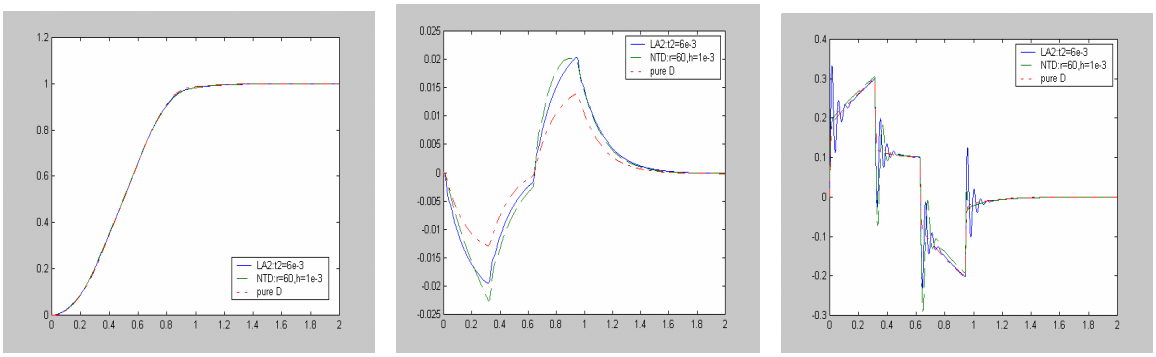

Position response Error response Control signal response

Figure 51. Comparing the normal responses when the NTD and LA2 are used

It's hard to tell which one is better from Figure 51, so the correlation coefficient was used again to evaluate the responses. The response of a pure differentiator is

considered as a reference. Table 10 shows the correlation coefficient of different differentiators to a pure differentiator for different responses.

Table 10. The comparing results when using the LA2 and NTD

	Position response	Error response	Control signal response
LA2-Pure D	1	0.9992	0.9740
NTD-Pure D	1	0.9940	0.9717

When the system is fed with measurement white noise (0.1%), the results are shown in Figure 52. No measurement noise input was applied to the pure differentiator, whose response is considered as a reference.

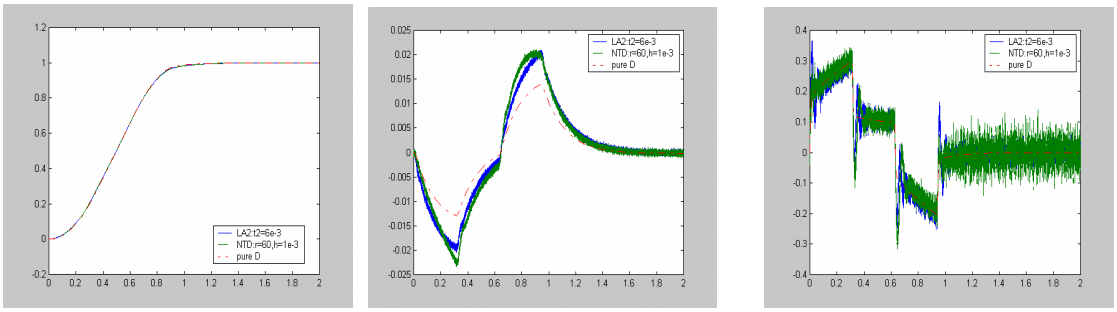

Position response Error response Control signal response

Figure 52. Comparing measurement noise responses when using the NTD and LA2

Correlation coefficient is used again to evaluate the responses in Table 11.

Table 11. The comparison results with measurement noise when using the LA2 and NTD

	Position response	Error response	Control signal response
LA2-Pure D	1	0.9987	0.9654
NTD-Pure D	1	0.9936	0.9447

Table 10 and Table 11 show that the second-order linear approximation differentiator has better performance. It has almost the same tracking performance as NTD. Moreover, it has the advantages of smaller error and better control signal.

CHAPTER VI

CONCLUSIONS

In the comparative study of differentiators, including the classical linear approximation differentiators, the nonlinear and linear Tracking Differentiators, first order Robust Exact Differentiator and observer-based differentiators, it was observed that the observer-based method (with linear or nonlinear gains) offers the best result in the absence of inaccuracies in the mathematical model of the plant. In the framework of practical constraints, with dynamic uncertainties in the plant, the second order linear approximation and the nonlinear tracking differentiator are practical solutions to differentiation. The second order linear approximation differentiator is simple in implementation. For double differentiators, the extended state observer provides best results in the presence of noise, followed by two cascaded second order linear approximation differentiators.

Among the Pure Integrator, Nonlinear Integrator, Clegg Integrator and Modified Nonlinear Integrator, the Clegg Integrator and Modified Nonlinear Integrator have the reset problem that disrupts the performance of the control system. Although the phase lag

of these integrators is smaller, it appears that their application is very limited. On the other hand, the Nonlinear Integrator demonstrates much better performance in simulation.

The above conclusions are drawn from numerical simulation of a practical control system where disturbance and noise are incorporated to make it realistic.

BIBLIOGRAPHY

[1] J. Han and W. Wang, “Nonlinear Tracking Differentiator”, *Systems Science and Mathematical Sciences,* Vol.14, No. 2, pp.177-183, 1994.

[2] B. Guo and J. Han, “A Linear Tracking-Differentiator and Application to the Online Estimation of the Frequency of a Sinusoidal Signal”, *Proceedings of the 2000 IEEE International Conference on Control Applications*, Anchorage, Alaska, September 25-27, 2000

[3] A. Levant, “Robust Exact Differentiation via Sliding Mode Technique”, *Automatica*, Vol. 34, No.3, pp.379-384, 1998.

[4] Zhiqiang Gao, “From Linear to Nonlinear Control Means: A Practical Progression”, Presented at the ISA Emerging Technology Conference, September 12, 2001; to appear in ISA Transactions.

[5] Pei S.-C. and J.-J. Shyu, "Eigenfilter Design of Higher-Order Digital Differentiators", *IEEE Trans. Acoust. Speech Signal Process.,* ASSP(37), pp505-511, 1989.

[6] Rabiner L. R. and K. Steiglitz, "The design of wide-band recursive and nonrecursive digital differentiators", *IEEE Trans. Audio Electroacoust*., AU(18), pp204-209,1970.

[7] Kumar B. and S. C. D. Roy, "Design of digital differentiators for low frequencies", *Proc. IEEE*, 76, pp287-289, 1988.

[8] Carlsson B., A. Ahlen and M. Sternad, "Optimal differentiation based on stochastic signal models", *IEEE Trans. Signal Process*., 39(2), pp341-353, 1991.

[9] J.Han, “Nonlinear design methods for control systems”, The Proc. of the 14th IFAC World Congress, Beijing, 1999.

[10] Steve Slavin, “Chances are: the only statistics book you’ll ever read”, Madison books, Lanham, NewYork, Oxford, 1998.

[11] Tomislav J. Stimac, “Digital Control of a 1-kW DC-DC switching Power converter”, 2000.

[12] N. Minorsky, "Directional stability and automatically steered bodies", J. Am. Soc. Nav. Eng. 34 (1922) 280.

[13] Jacob Tal, “Motion Control System”, The Control Handbook. Editor Williams S. Levine, pp. 1382-1386, CRC Press and IEEE Press, 1995.

[14] Zhiqiang Gao, “Scaling, Parameterization and Optimization: Reinventing the Art of SISO Control Design”

[15] Zhiqiang Gao, Shahua Hu, “A Novel Motion Control Design Approach Based on Active Disturbance Rejection”, *Proceedings of the 40th IEEE conference on Decision and Control*, Orlando, Florida, USA, December 2001.

[16] Tomislav J.Stimac, “Digital Control of a 1-kW DC-DC switching Power converter”, Master Thesis, Department of Electrical and Computer Engineering, Cleveland State University, December 2000.

[17] Clegg, J.C., “A Nonlinear Integrator for Servomechanisms”, *Trans. A.I.E.E.*, part II, Vol.77, pp41-42, 1958.

[18] J. Han, Manuscript “PID and Tracking Differentiator”.

[19] Minshao Zhu, “A Nonlinear Digital Control Solution for a DC/DC Power converter”, Master Thesis, Department of Electrical and Computer Engineering, Cleveland State University, February 2002.

[20] Zhiqiang Gao, “An Alternative Paradigm for Control System Design”, *IEEE Conference on Decision and Control,* 2001

[21] B. T. Boulter, “Applying Drive Specifications to System Applications: Part III Position Regulation”, IEEE IAS Annual Meeting, 2002